

Neurovascular anatomy of the protostegid turtle *Rhinochelys pulchriiceps* and comparisons of membranous and endosseous labyrinth shape in an extant turtle

SERJOSCHA W. EVERS^{1,2*}, JAMES M. NEENAN³, GABRIEL S. FERREIRA^{4,5},
INGMAR WERNEBURG^{5,6}, PAUL M. BARRETT² and ROGER B. J. BENSON¹

¹Department of Earth Sciences, University of Oxford, South Parks Road, Oxford OX1 3AN, UK

²Department of Earth Sciences, Natural History Museum, Cromwell Road, London SW7 5BD, UK

³Oxford University Museum of Natural History, Parks Road, Oxford OX1 3PW, UK

⁴Faculdade de Filosofia, Ciências e Letras de Ribeirão Preto, Universidade de São Paulo, Av. Bandeirantes 3900, 14040-901 Ribeirão Preto, Brazil

⁵Fachbereich Geowissenschaften der Eberhard-Karls-Universität Tübingen, Hölderlinstraße 12, 72074 Tübingen, Germany

⁶Senckenberg Center for Human Evolution and Palaeoenvironment (HEP) an der Eberhard Karls Universität, Sigwartstraße 10, 72076 Tübingen, Germany

Received 26 March 2019; revised 27 May 2019; accepted for publication 9 June 2019

Chelonioid turtles are the only surviving group of reptiles that secondarily evolved marine lifestyles during the Mesozoic. Early chelonioid evolution is documented by fossils of their stem group, such as protostegids, which yield insights into the evolution of marine adaptation. Neuroanatomical features are commonly used to infer palaeoecology owing to the functional adaptation of the senses of an organism to its environment. We investigated the neuroanatomy and carotid circulation of the early Late Cretaceous protostegid *Rhinochelys pulchriiceps* based on micro-computed tomography data. We show that the trigeminal foramen of turtles is not homologous to that of other reptiles. The endosseous labyrinth of *R. pulchriiceps* has thick semicircular canals and a high aspect ratio. Comparisons among turtles and other reptiles show that the endosseous labyrinth aspect ratio is not a reliable predictor of the degree of aquatic adaptation, contradicting previous hypotheses. We provide the first models of neuroanatomical soft tissues of an extant turtle. Turtle brain morphology is not reflected by the brain cavity, and the endosseous labyrinth provides an incomplete reflection of membranous semicircular duct morphology. Membranous labyrinth geometry is conserved across gnathostomes, which allows approximate reconstruction of the total membranous labyrinth morphology from the endosseous labyrinth despite their poor reflection of duct morphology.

ADDITIONAL KEYWORDS: brain morphology – marine adaptation – neuroanatomy – palaeoecology – sea turtles – sensory evolution – trigeminal nerve – vestibular organ.

INTRODUCTION

The increased availability of computed tomography for palaeontological research has facilitated many studies describing the internal cranial anatomy of fossil turtles, including osteology (e.g. Brinkman *et al.*, 2006; Lipka *et al.*, 2006; Sterli *et al.*, 2010; Jones *et al.*, 2012; Bever *et al.*, 2015; Evers *et al.*, 2019), neurosensory anatomy

(Walsh *et al.*, 2009; Carabajal *et al.*, 2013, 2017; Willis *et al.*, 2013; Ferreira *et al.*, 2018; Lautenschlager *et al.*, 2018) and vascular anatomy (e.g. Joyce *et al.*, 2018; Myers *et al.*, 2018; Rollet *et al.*, 2018). Besides the comparative anatomical and phylogenetic value of these data (e.g. Evers & Benson, 2019), neuroanatomical reconstructions based on osteological correlates of respective tissues have received attention, because they provide the potential to infer the neurological capabilities and palaeoecologies of extinct taxa (e.g. Witmer *et al.*, 2003; Walsh *et al.*, 2009; Rowe *et al.*, 2011;

*Corresponding author. E-mail: serjoscha.evers@googlegmail.com

Balanoff *et al.*, 2013; Yi & Norell, 2015; Neenan *et al.*, 2017; Lautenschlager *et al.*, 2018). Neuroanatomical structures can be reconstructed digitally as three-dimensional (3D) endocast models when the respective organs are housed in bony cavities of the skull (Witmer *et al.*, 2008; Balanoff *et al.*, 2015; see Fig. 1). These endocasts of the brain cavity represent the brain and cranial nerves (CNs), in addition to the endocast of the endosseous labyrinth of the inner ear, and have been used both qualitatively and quantitatively to interpret the neurological capabilities and palaeoecology of individual turtle taxa (e.g. Lautenschlager *et al.*, 2018) and to observe and interpret the sensory evolution and palaeoecology of larger clades (e.g. Thewissen & Nummela, 2008).

Here, we present digital endocasts of the brain cavity and endosseous labyrinth of the early Late Cretaceous protostegid turtle *Rhinochelys pulchriiceps* (Owen, 1851) from high-resolution X-ray micro-computed-tomography (μ CT) data (see Fig. 1). The phylogenetic position of protostegids has been disputed (e.g. Hirayama, 1998; Hooks, 1998; Joyce, 2007; Cadena & Parham, 2015; Raselli, 2018; Evers & Benson 2019; Evers *et al.*, 2019), but all global phylogenetic studies that include more than one protostegid recover them as total-group chelonoids (e.g. Cadena & Parham, 2015; Raselli, 2018; Evers & Benson, 2019; Evers *et al.*, 2019). Despite uncertainties about their exact phylogenetic position with respect to crown-group sea

turtles (see Raselli, 2018; Evers & Benson, 2019; Evers *et al.*, 2019), protostegids represent early members of the only turtle lineage that evolved a pelagic lifestyle. Early protostegids, such as *Rhinochelys*, lack several of the derived traits of the flippers seen in crown-group chelonoids and the leatherback sea turtle, *Dermochelys coriacea* (Linnaeus, 1766) (e.g. Hirayama, 1998; Tong *et al.*, 2006; Evers *et al.*, 2019), suggesting that they were not fully pelagic. Being stem taxa of either *Dermochelys coriacea* or chelonoids, protostegids provide morphological data on the evolution of marine adaptation in sea turtles.

One of our goals is to examine the osteological correlates for neuroanatomy, such as the endocast of the brain cavity and particularly the structure of the endosseous labyrinth of *R. pulchriiceps*. Observations from *R. pulchriiceps* can provide insights into the neuroanatomical evolution of secondarily marine turtles and will help in developing hypotheses about whether, and how, neuroanatomical changes are correlated with ecological transitions, such as the evolution of a pelagic lifestyle in chelonoids.

Our study reveals several important comparative aspects of the turtle endosseous labyrinth (the bony chamber that houses the vestibular organ), including the semicircular canals. The semicircular canals contribute to sensory control of gaze stabilization by detecting angular accelerations of the head as inputs to the vestibulo-ocular and vestibulo-colic reflexes (Spoor & Zonneveld, 1998). Membranous labyrinth geometry determines the dynamics of internal endolymphatic fluid flow and has a hypothesized relationship to sensitivity of the vestibular organ to different vectors of angular acceleration (i.e. semicircular canals) and linear accelerations (i.e. utricle and saccule) (e.g. Wilson & Melville Jones, 1979). Therefore, the shape of the vestibular organ should vary depending on locomotor mode (e.g. Spoor *et al.*, 2007; Pfaff *et al.*, 2015, 2017). In order to investigate the correspondence of the endocasts of the brain cavity and the brain, in addition to the endosseous and membranous labyrinth shape in turtles, we produced digital models of these structures from scans of a wet specimen of an extant aquatic (but non-marine) turtle, *Trachemys scripta* (Thunberg in Schoepff, 1792), and used it as a guide for interpreting the endocranial morphology of *R. pulchriiceps*, which is known only from fossils that lack soft tissue.

We also described the carotid arterial pattern of *R. pulchriiceps* by describing endocasts of the bony canals that serve as osteological correlates for the arteries. The carotid arterial system of turtles has received considerable attention (e.g. McDowell, 1961; Albrecht, 1967, 1976; Gaffney, 1975a; Jamniczky & Russel, 2007; Jamniczky, 2008; Sterli & De la

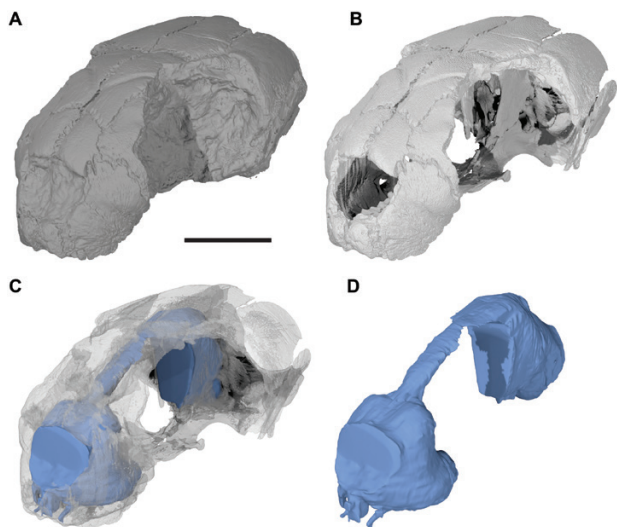


Figure 1. *Rhinochelys pulchriiceps* (CAMS B55775) in anterodorsolateral view. A, three-dimensional (3D) rendering of the complete specimen. B, 3D rendering of the cranium, with matrix removed. C, transparent 3D rendering of the cranium with solid model of the brain cavity inside. D, 3D rendering of the brain cavity endocast. Scale bar: 10 mm.

Fuente, 2010; Sterli *et al.*, 2010; Müller *et al.*, 2011; Miyashita, 2012; Rabi *et al.*, 2013), particularly because different patterns have been interpreted as phylogenetically informative. Rabi *et al.* (2013) proposed a comprehensive and internally consistent nomenclatural system for the canals and foramina associated with the carotid arterial system, which facilitates comparative research regarding the carotid arterial system. The arterial pattern and, more specifically, the topological position of foramina, the ossification of basicranial elements encasing the arteries in bone, and the course of the canals through the basicranium may not only be informative for turtle in-group relationships, but might also yield wider phylogenetic information about the position of turtles within amniotes (e.g. Sterli *et al.*, 2010; Müller *et al.*, 2011; Rabi *et al.*, 2013). The description of the carotid arterial systems for fossil turtles is therefore important. Although aspects of the carotid arterial system of protostegids have been described (e.g. Hooks, 1998: *Calcarichelys gemma* Zangerl, 1953; *Protostega gigas* Cope, 1872), the present work represents the first detailed carotid arterial description and first clear 3D visualization of this system in a protostegid.

MATERIAL AND METHODS

INSTITUTIONAL ABBREVIATIONS

AMNH, American Museum of Natural History, New York City, NY, USA; CAMSM, Sedgwick Museum of Earth Sciences, Cambridge, UK; FMNH, Field Museum of Natural History, Chicago, IL, USA; NHMUK, Natural History Museum London, London, UK; SMF, Senckenberg Museum Frankfurt, Frankfurt, Germany; UMZC, University Museum of Zoology, Cambridge, UK.

TOMOGRAPHIC DATA USED IN THIS STUDY

Evers *et al.* (2019) published a taxonomic revision and osteological description of *R. pulchriceps* based on μ CT scans of six specimens, and we used these data, which are deposited in the online database MorphoSource (Evers & Benson, 2018; Evers *et al.*, 2018). Given that the arterial pattern, endosseous labyrinth shape, paths of nerves and the cranial endocast shape were consistent between all six specimens of *R. pulchriceps*, we use only two specimens herein, which were the best preserved, to illustrate various aspects of the neuroanatomy, basicranium and vascular system. For the arterial system, we used CAMSM B55783, which was μ CT scanned at a resolution of 20.4 μ m (isometric voxel size), with the following settings: 215 kV, 200 μ A, 1 mm Cu (Copper) filter and 708 ms exposure time.

CAMSM B55775 (Fig. 1), the holotype specimen of *R. pulchriceps*, was used to illustrate the cranial endocast, cranial nerves and endosseous labyrinth. This specimen was scanned at a resolution of 35.5 μ m (isometric voxel size), 205 kV, 195 μ A, 1 mm Cu filter and 708 ms exposure time. The scanning parameters are also deposited at MorphoSource with the slice and model data (CAMSM B55783, Evers & Benson, 2018; CAMSM B55775, Evers *et al.*, 2018). Three-dimensional models were generated through manual segmentation in the software MIMICS v.16.0–18.0 (<http://biomedical.materialise.com/mimics>) and exported as PLY files. We used the software BLENDER v.2.71 (blender.org) to compile figures of digital renderings.

The *T. scripta* micro-magnetic resonance imaging (μ MRI) scan data were shared with us by Gilles Laurent, who acquired the images using a vertical-bore 11.7 T Bruker Avance DRX500 system (Bruker BioSpin Inc., Billerica, MA, USA) equipped with a Micro 2.5 gradient system, using a 35 mm linear birdcage radio frequency (RF) foil. A 3D FLASH imaging sequence was used, and the following scan parameters were used: repetition time, TR = 80 ms; effective echo time, TE_{eff} = 7.8 ms; four averages and a 39 μ m isotropic voxel size. The *T. scripta* (no specimen number available; J.M.N. pers. comm. to Gilles Laurent) was euthanized according to Caltech IACUC protocol #1576-08 to Gilles Laurent, and the head of the animal was fixed in 4% paraformaldehyde (PFA) and then soaked in 5 mM ProHance for 8 days before imaging.

RESULTS

VASCULAR AND NEUROANATOMICAL DESCRIPTION OF *R. PULCHRICEPS* AND COMPARISON WITH OTHER TURTLES

Arterial circulation

In turtles (Albrecht, 1976; Müller *et al.*, 2011) and in other reptiles, including birds (Porter & Witmer, 2015; Porter *et al.*, 2016), the stapedia artery branches off the internal carotid artery. The internal carotid artery then enters the basicranium through the foramen posterius canalis carotici interni (fpcci; all foramina and canal terminology follows Rabi *et al.*, 2013; Fig. 2). The position of this foramen and the bones that form its margins vary among turtles (e.g. Joyce, 2007; Sterli & De la Fuente, 2010; Rabi *et al.*, 2013). In *R. pulchriceps*, the fpcci is located on the sutural contact between the parabasisphenoid and pterygoid, immediately anterior to the posterior process of the latter (Fig. 2C, D). This position of the fpcci is common to all protostegids for which the foramen is visible (e.g. Hooks, 1998; Cadena

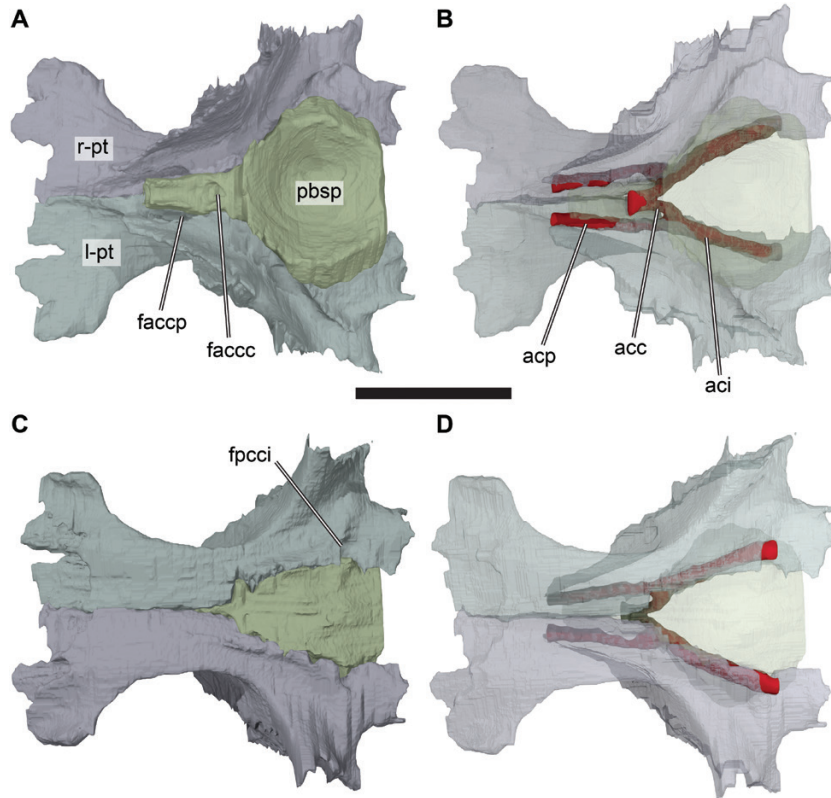


Figure 2. Carotid arterial system and associated features of *Rhinochelys pulchriceps* (CAMSM B55783) illustrated by three-dimensional renderings of parts of the basicranium. A, B, dorsal view. C, D, ventral view. In A, C, partial basicranium is rendered solid, with different colours given to all included bones. In B, D, partial basicranium is rendered transparent, and reconstructed carotid arterial system is shown in red. Abbreviations: acc, cerebral artery; aci, internal carotid artery; acp, palatine artery; faccc, foramen anterius canalis carotici interni; faccp, foramen anterius canalis carotici palatinum; fpcci, foramen posterior canalis carotici interni; l-pt, left pterygoid; pbsp, parabasisphenoid; r-pt, right pterygoid. Scale bar: 5 mm.

& Parham, 2015; Evers & Benson, 2019) and is also observed in *Dermochelys coriacea* (Evers & Benson, 2019) and at least some plesiochelyids (Gaffney, 1975b; Anquetin *et al.*, 2015; Evers & Benson, 2019). Extant chelonids have their fpcci entirely positioned in the pterygoid (Evers & Benson, 2019), and a pterygoid contribution to the foramen is common to all cryptodires, but also likely to be the plesiomorphic state for turtles (Evers & Benson, 2019). The canalis carotici interni of *R. pulchriceps* continues anteriorly between the pterygoid and parabasisphenoid and diverges into a lateral and a medial canal inside the cranium immediately posterior to the level of the base of the rostrum basisphenoidale (Fig. 2B, D). The lateral canal is interpreted as the canalis caroticus palatinum, which would have housed the palatine artery (e.g. Rabi *et al.*, 2013). In *R. pulchriceps*, this canal continues anteriorly and is bounded medially by the rostrum basisphenoidale of the parabasisphenoid, but is otherwise enclosed by the pterygoid (Fig. 2B, D). Anteriorly, the palatine canal ends in the foramen

anterius canalis carotici palatinum (Rabi *et al.*, 2013), which is positioned ventral to the level of the sulcus olfactorius and about halfway along the length of the rostrum basisphenoidale in *R. pulchriceps* (Fig. 2A). The second, medial branch of the internal carotid artery is the cerebral artery (e.g. Müller *et al.*, 2011; Rabi *et al.*, 2013), which is contained in a short, bony canal in all known shelled turtles (i.e. including *Proganochelys quenstedti* Baur, 1887; Gaffney, 1990). In *R. pulchriceps*, the canal for the cerebral artery projects in an anteromedial and dorsal direction into the parabasisphenoid (Fig. 2B, D). Left and right cerebral arteries have separate posterior courses, but join to run through a single, median canalis caroticus cerebialis within the parabasisphenoid more anteriorly (Fig. 2B). The canalis caroticus cerebialis opens anteriorly within the sella turcica on the dorsal surface of the rostrum basisphenoidale via a single, large foramen anterius canalis carotici cerebialis (Fig. 2A, B). The shared anterior canal for the right and left cerebral arteries is an unusual feature with respect to

other turtles, which until recently had been reported in the protostegids *Calcarichelys gemma* Hooks, 1998, *Protostega gigas* Hooks, 1998 and *Notochelone costata* (Owen, 1882) only (Evers *et al.*, 2019). However, this condition is also present in some cheloniids, such as *Lepidochelys olivacea* (Eschscholtz, 1829) (Evers & Benson, 2019: character 142 discussion). In most other turtles, the left and right cerebral canals open into the parabasisphenoid through separate openings, which can vary from closely spaced (as in most cheloniids; e.g. Hirayama, 1998; Myers *et al.*, 2018) to widely separated positions (as in most other turtles; Hirayama, 1998; Cadena & Parham, 2015; Evers & Benson, 2019).

The dorsal part of the course of the stapedia artery can be traced in *R. pulchriceps* vertically through the canalis stapedio-temporale between the quadrate and prootic, as in most turtles (Gaffney, 1979). Its exact course through the cavum acustico-jugulare cannot be reconstructed, but it is usually parallel with and dorsal to the vena capitis lateralis, which extends along the floor of the cavum acustico-jugulare and canalis cavernosus in extant turtles (Gaffney, 1979). Assuming that a cryptodire-like arterial circulation was present (Albrecht, 1976; Gaffney, 1979), the mandibular artery in *Rhinochelys* would have branched off the stapedia artery within the cavum acustico-jugulare, exiting into the fossa subtemporalis through the ('external'; see below) trigeminal foramen.

Cranial endocast

CAMSM B55775 (Fig. 3) was selected for the cranial endocast reconstruction because its braincase is completely preserved, including the posterior elements, and the nasal capsule is also preserved. Following the description of *Plesiochelys etalloni* Pictet & Humbert, 1857 provided by Carabajal *et al.* (2013), the endocast of the nasal capsule has been included in the endocast of *Rhinochelys*.

Turtle endocasts represent only the gross morphology of the brain, for several reasons discussed below. Brains of modern non-avian reptiles are much smaller than their respective endocranial cavities (Hopson, 1979), and the resulting size (volume) difference between the brain cavity and the brain has been reported to be particularly large in turtles (Edinger, 1929; Zangerl, 1960), which is also evident from our work on *T. scripta* (see section 'Brain morphology, cranial nerves and comparisons with the brain cavity in *T. scripta*'). However, the differences in shape between the brain cavity and brain tissue have not been analysed for turtles. A dural envelope surrounds the turtle brain, and subdural and epidural spaces exist in extant sea turtles (Wyneken, 2001), which further minimize the

correspondence between the brain tissue and brain cavity. This affects size differences but probably also shape differences between turtle brain cavities and their brain morphologies. Although, to our knowledge, this has not been stated explicitly, endocasts of turtle brain cavities lack distinct separations between, for instance, the optic lobe and cerebrum (e.g. Lautenschlager *et al.*, 2018), whereas these structures are distinct in published images of turtle brains (e.g. Wyneken, 2001) and *T. scripta* (see section 'Brain morphology, cranial nerves and comparisons with the brain cavity in *T. scripta*').

In addition, the turtle braincase is peculiar in possessing a secondary lateral braincase wall anterior to the prootic, which is formed by the processus inferior parietalis of the parietal (Gaffney, 1979; Werneburg & Maier, 2019). A primary lateral braincase wall anterior to the prootic, which is commonly ossified as the laterosphenoid in archosauriforms (e.g. Holliday & Witmer, 2007; Bhullar & Bever, 2009), is absent in most turtles (Werneburg & Yaryhin, 2018). Consequently, the primary brain cavity is laterally expanded beyond the parabasisphenoid cup and extends dorsally over the sulcus cavernosus to include the cavum epiptericum. The cavum epiptericum houses the trigeminal ganglion (Soliman, 1964; Starck, 1979; Holliday & Witmer, 2007) and is generally an extracranial space that becomes enclosed within the laterally expanded brain cavity in turtles (Starck, 1979). However, a membranous wall and possibly some cartilaginous remainders separate the cavum epiptericum from the brain cavity *s.s.* (Starck, 1979).

Carabajal *et al.* (2013) included both the sulcus cavernosus and the cavum epiptericum in their digital endocast of *Plesiochelys etalloni*. However, for *R. pulchriceps* we excluded both structures. As a result of this, the pituitary is visible as a protuberance on the ventral surface of the endocast (Fig. 3B, C), as also shown by Lautenschlager *et al.* (2018) (rather than as a depression between the sulci cavernosi). This is a more accurate representation of the pituitary than that provided by Carabajal *et al.* (2013), because our model fills the sella turcica to the exclusion of the ventrally underlying rostrum basisphenoidale, whereas the depression between the sulci cavernosi includes both the depth of the pituitary and the rostrum basisphenoidale. Our rendering of the trigeminal nerve (Fig. 3B, C) includes most of the space within the cavum epiptericum (i.e. the trigeminal ganglion is segmented as part of the nerve masks, rather than part of the endocast).

In spite of the above-mentioned difficulties regarding the reliability of turtle brain cavities as indicators of brain shape, several general statements can be made, which include the passages of those cranial nerves that

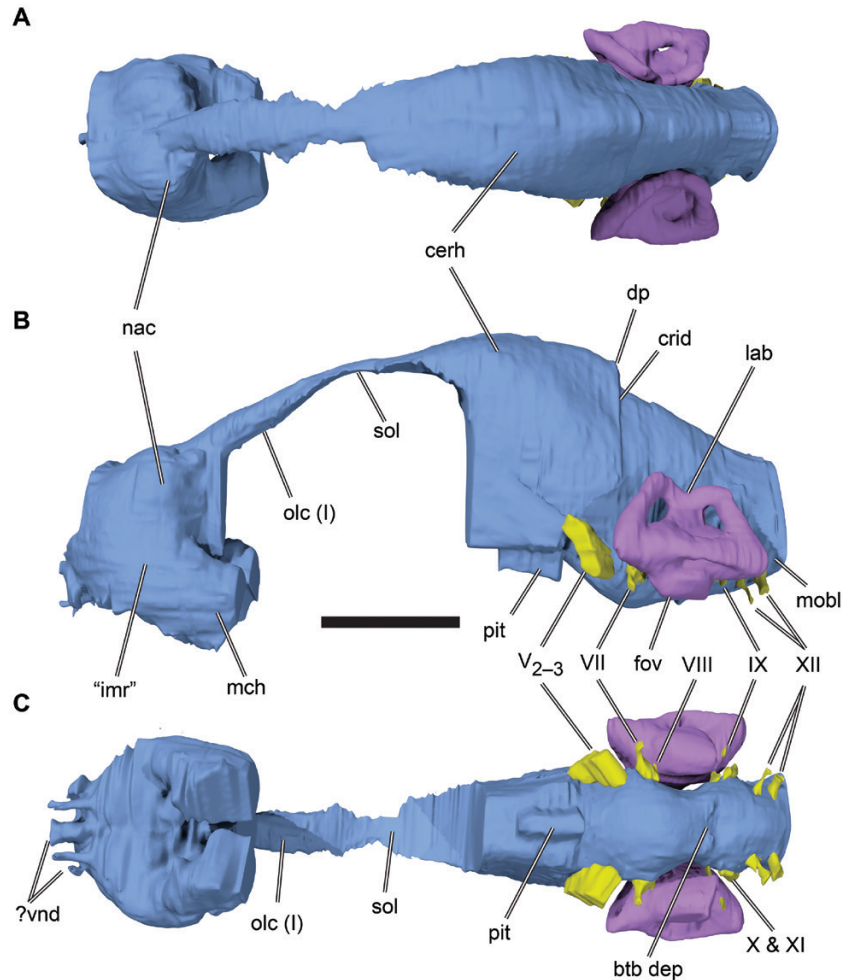


Figure 3. Endocranial morphology of *Rhinochelys pulchriceps* (CAMSM B55775) illustrated by three-dimensional renderings. A, dorsal view. B, left lateral view. C, ventral view. Abbreviations: btb dep, basis tuberculi basalis depression; cerh, cerebral hemisphere; crid, cartilaginous rider; dp, dural peak; fov, fenestra ovalis; imr, intermediate region; IX, glossopharyngeal nerve (cranial nerve IX); lab, endosseous labyrinth; mch, meatus choane; mobl, medulla oblongata; nac, nasal capsule; olc, olfactory canal; pit, pituitary fossa; sol (I), sulcus olfactorius, including olfactory nerve (cranial nerve I); V2–3, maxillomandibular division of the trigeminal nerve (cranial nerve V2–3); VII, facial nerve (cranial nerve VII); VIII, vestibulocochlear (= statoacustico) nerve (cranial nerve VIII); vnd, vomeronasal diverticulae; X, vagus nerve (cranial nerve X); XI, accessory nerve (cranial nerve XI); XII, hypoglossal nerves (cranial nerve XII). Scale bar: 10 mm.

are contained by bone, in addition to brain flexures (e.g. Lautenschlager *et al.*, 2018). The canals for the cranial nerves for *R. pulchriceps* have been described briefly (Evers *et al.*, 2019), but this information is summarized here to provide an inclusive description of the endocast and its associated neural structures.

Although the endocast of *R. pulchriceps* is principally tubular (Fig. 3A, B), it is more strongly flexed than in *Plesiochelys etalloni* (Carabajal *et al.*, 2013) or *Proganochelys quenstedti* (Lautenschlager *et al.*, 2018), but not as strongly as in *Meiolania platyceps* Owen, 1886 (Carabajal *et al.*, 2017). The cephalic flexure between the forebrain and hindbrain is much more strongly developed than in *Plesiochelys*

etalloni and mirrors the form of modern cheloniids (see images provided by Zangerl, 1960) and also *Dermochelys coriacea* (as evident from parasagittally sectioned braincases; Nick, 1912). The cerebral area and olfactory lobe area form a continuously curved, convex shape (Fig. 3B). However, the olfactory lobes are not discernible in *R. pulchriceps*, whereas they have been identified in *Plesiochelys etalloni* as small, weakly convex structures lying anteromedial to the cerebral hemispheres (Carabajal *et al.*, 2013).

The forebrain of *R. pulchriceps* extends anteroventrally from the cephalic flexure as a cast of the sulcus olfactorius ventral to the frontals. The anterior extent of the olfactory bulbs cannot be

distinguished from the course of the olfactory nerves, which are anteroventrally directed from them. The anterior part of the olfactory nerve path is well defined by the olfactory canal, which is formed by ventrally fused cristae cranii. An osseous olfactory canal has so far been identified only in the protostegids *R. pulchriceps* and *N. costata* (Evers & Benson, 2019; Evers *et al.*, 2019) and is not present in either other turtles or other protostegids, such as *Desmatochelys lowii* Williston, 1894 (Raselli, 2018; S.W.E., pers. obs.) and *Bouliachelys suteri* Kear & Lee, 2006 (Evers & Benson, 2019). Anteriorly, the olfactory canal of *R. pulchriceps* enters the nasal cavity above the fissura ethmoidalis. The fissura ethmoidalis is visible as a narrow, 'V'-shaped median structure on the posterior surface of the nasal cavity.

The nasal cavity itself is dorsolaterally expanded and forms a strongly convex hemisphere on either side of the skull midline (Fig. 3). It is in this dorsal part that the olfactory epithelium of the olfactory sacs lies (Wyneken, 2001; Schwenk, 2008). In the dorsal part of the nasal cavity, left and right nasal valves, which would be separated in life by the median, vertically oriented internarial septum, can be distinguished by a shallow median sulcus (Fig. 3A). Ventrally, this division is also discernible from a median groove in the endocast of the nasal cavity (Fig. 3C), which is the imprint of the median ridge shared between the premaxillae anteriorly and vomer posteriorly. Although the nasal capsule is a large chamber, it is not as large as in the stem-group turtles *Proganochelys quenstedti* or *M. platyceps* (Carabajal *et al.*, 2017; Lautenschlager *et al.*, 2018).

Anterodorsally, the nasal cavity opens via a single external naris in *R. pulchriceps*. Ventral to the external naris, the nasal capsule extends anteriorly to form a short, bulbous hemisphere (Fig. 3B), termed the 'intermediate region' (Parsons, 1970; Schwenk, 2008), which houses vomeronasal epithelium in sea turtles (Parsons, 1970; Wyneken, 2001; Schwenk, 2008). The 'intermediate region' of *R. pulchriceps* extends anteriorly into the interpremaxillary suture, a feature that is visible in the endocast as a vertically oriented median ridge, located anteriorly and bearing a centrally placed, anteriorly directed short tubular protuberance. It is possible that this anterior cavity positioned between the premaxillae is associated with the vomeronasal organ. Short, paired lateral canals extend anteroventrally through the premaxilla either side of the 'intermediate region', extending to the triturating surface of the palate (Fig. 3C). The identity of these canals is unclear; it is possible that they represent vascular canals, but they might also be related to the vomeronasal organ. The vomeronasal epithelium in sea turtles is sequestered into dorsal and ventral diverticulae from the intermediate region

(Parsons, 1970; Schwenk, 2008), and the ventral extensions seen in *R. pulchriceps* are in accordance with this morphology.

The anterodorsal portion of the forebrain is narrow, and the olfactory bulbs are not discernible in *R. pulchriceps*. The cerebral hemispheres of the forebrain are visible in *R. pulchriceps* as shallow convexities on the dorsolateral surface of the endocast to either side of its midline (Fig. 3A). The anterior surface of the forebrain in *R. pulchriceps* is segmented until the anterior end of the processus inferior parietalis, resulting in a flat surface ventral to the anteriorly extending olfactory tract. The vertical anterior end of the brain cavity results in a large interorbital fenestra, which has been interpreted as being indicative of well-developed salt glands (Hirayama, 1998). The large interorbital fenestrae in *R. pulchriceps* are consistent with the morphology of *Dermochelys coriacea*, for instance, which has particularly large salt glands (Wyneken, 2001). Furthermore, this morphology is widely present among chelonoids and differs from the condition in other cryptodires, including amechelydians such as *Sternotherus minor* Agassiz, 1857 (FMNH 211696; Evers & Benson, 2018). However, large interorbital fenestrae are also present in clearly terrestrial turtles (e.g. Meiolaniformes; Gaffney, 1983, 1992), meaning that a close form–function relationship between large interorbital fenestrae and the presence of large salt glands cannot be inferred. Furthermore, the salt gland of *Dermochelys coriacea* is situated laterally in the head, posterior to the eye and not medially to it (Schumacher, 1972), where the interorbital septum is located. Developmental data additionally show that only small true interorbital fenestrae develop during ontogeny and that a thin membrane as a remainder of the cartilaginous interorbital septum remains even in adult turtles (Tulenko & Sheil, 2007; see also Yaryhin & Werneburg, 2018). Therefore, the occurrence of large interorbital fenestrae in chelonoids is likely not to be related directly to the presence of salt glands.

The anterior surface of the midbrain region between the anterior margins of the parietals is unossified in turtles (with the possible exception of *Proganochelys quenstedti*; Bhullar & Bever, 2009; but see Lautenschlager *et al.*, 2018; Werneburg & Yaryhin, 2018), meaning that the foramina for cranial nerves II–IV are not encased in bone and cannot be represented in the digital endocast of *R. pulchriceps*, as is also the case in *Plesiochelys etalloni* (Carabajal *et al.*, 2013).

The portion of the midbrain posterior to the cephalic flexure is posteroventrally directed (Fig. 3A). The ventral part of the midbrain in *R. pulchriceps* is marked by a narrow, longitudinal protrusion, which represents the digital infill of the sella turcica (Fig. 3B, C).

This protrusion includes the pituitary gland, but almost certainly overestimates its size, because the sella turcica is not usually filled completely by neural tissue (Hopson, 1979; also see *T. scripta*, below). The cast of the pituitary is posteriorly confluent with the foramen arterius canalis carotici cerebri, through which the cerebral artery exits the parabasisphenoid. Posterolateral to the pituitary, the abducens nerve (CN VI) exits the cranial cavity through small, paired foramina near the base of the clinoid processes. In CAMSM B55775, these nerves have not been segmented because their respective canals are not visible in the μ CT scans, but other specimens show that the CN VI canals are short, anteroposteriorly oriented structures (Evers *et al.*, 2019: fig. S1.19).

The most distinctive feature of the mid- to hindbrain region in *R. pulchriceps* is a transversely oriented step between the surface of the posterior portion of the midbrain and the metencephalon of the hindbrain. This step is dorsally hypertrophied by a centrally placed eminence, the dural peak, but is also visible laterally as a vertical step dorsal to the posterior level of the trigeminal nerve (Fig. 2B). This transverse ridge is the margin of the ‘cartilaginous rider’ of Zangerl (1960), who described this feature first in an endocast of the chelonoid *Corsochelys halinches* Zangerl, 1960 and who also found this structure in modern cheloniid endocasts. The cartilaginous rider is a triangular, slightly dorsally elevated area on the dorsal surface of the midbrain region of endocasts in these turtles (Zangerl, 1960). It narrows anteriorly between the cerebral hemispheres. Zangerl (1960) interpreted the cartilaginous rider as a cartilaginous anterior extension of the supraoccipital, a view that was adopted by Hopson (1979). In addition to its presence in *C. halinches* and modern cheloniids, it has also been identified in *Plesiochelys etalloni* (Carabajal *et al.*, 2013), various fossil bothremydid (Gaffney & Zangerl, 1968) and podocnemidid (Ferreira *et al.*, 2018) pleurodires and in stem turtles (e.g. Carabajal *et al.*, 2017; Lautenschlager *et al.*, 2018). However, in pleurodires the rider forms a narrow, vaguely tubular dorsal protrusion of the endocast, rather than a low triangular area with well-delimited posterior and posterolateral borders. Carabajal *et al.* (2013) explained the presence of the lateral, ridge-like demarcations of the rider and its alignment with the ventrally adjacent (‘external’; see below) trigeminal (CN V₂₋₃) foramen in *Plesiochelys etalloni* as indicators for the course of the dorsal head vein and rostral cerebral vein. However, the posterior border of the rider in *R. pulchriceps* is clearly an artefact of the anterior margin of the supraoccipital; the supraoccipital ends anteriorly at the level of the position of the trigeminal nerve and, anterior to this point, the roof of the brain cavity is formed by the parietals, which overlie the dorsal

surface of the supraoccipital. Unless the anterior end of the supraoccipital coincides with the course of the dorsal head vein and the rostral cerebral vein, the cartilaginous rider appears to be unrelated to either the central nervous system or associated vascular structures, supporting the original proposal of Zangerl (1960). This is supported by our observations on *T. scripta*, in which we did not find evidence for veins associated with the brain lying directly against the inner bony braincase wall. However, the dorsally hypertrophied dural peak in the posterodorsal border of the cartilaginous rider seen in *R. pulchriceps* seems to represent a genuine feature; if the endocast of *R. pulchriceps* is posteriorly segmented to include the anterior parts of the supraoccipital, the lateral ridges of the rider vanish, whereas a small dorsal convexity remains. This is consistent with other studies in which the dural peak is present, whereas lateral demarcations of the cartilaginous rider are absent (e.g. Lautenschlager *et al.*, 2018).

Wyneken (2001) has shown that the pineal gland of chelonoids extends dorsally from the brain into the region of the dural peak and that the pineal gland connects to the skull roof in *Dermochelys coriacea*. We also observed the pineal gland of *T. scripta* in this region of the brain (see section ‘Brain morphology, cranial nerves and comparisons with the brain cavity in *T. scripta*’). The presence of a well-developed pineal organ has also been proposed for the protostegid *Desmatochelys lowii* (Raselli, 2018). *Desmatochelys lowii* and *Desmatochelys padillai* Cadena & Parham, 2015 show evidence for the presence of a pineal foramen, although the pineal foramen of *Desmatochelys lowii* has recently been reinterpreted as breakage (Raselli, 2018). Nevertheless, a pineal foramen is present in several specimens of *Desmatochelys padillai* (Cadena & Parham, 2015). In several well-preserved *R. pulchriceps* specimens (e.g. CAMSM B55783; Evers *et al.*, 2019), the anterior part of the parietals is damaged, indicating that this area of the skull roof was possibly thinner than other parts. It is difficult to determine whether the dural peak of *R. pulchriceps* provides evidence of a pocket for the pineal gland similar to that of *Dermochelys coriacea*.

The metencephalic part of the hindbrain (anterior to the pontine flexure) continues to be posteroventrally directed posterior to the cartilaginous rider (Fig. 3B). Its ventrolateral side is marked by the origins of cranial nerves V and VII + VIII. The nerve stem for the trigeminal nerve (CN V) exits the primary cranial cavity dorsal to the anterolateral margin of the basisphenoid cup, posterior to the clinoid process and anterior to the prootic. It extends into the cavum epiptericum and forms a single ganglion (Starck, 1979). The ophthalmic (V₁) ramus of the trigeminal nerve diverges anteriorly from this ganglion and medially to the secondary

lateral wall of the braincase formed by the processus inferior parietalis, but leaves no osteological trace. Only the maxillomandibular rami (V_{2-3}) of the trigeminal complex exit into the subtemporal or adductor fossa (= fossa temporalis inferior *sensu* Gaffney, 1972) through the foramen between the parietal, pterygoid and prootic. This foramen is commonly referred to as the trigeminal foramen (e.g. Gaffney, 1979), but given that it is not homologous with the trigeminal foramen of other reptiles, as we discuss below, we use the term 'external' trigeminal foramen for this description.

Slightly posterior to the 'external' trigeminal foramen, the facial (CN VII) and vestibulocochlear (CN VIII) nerve foramina exit the cranial cavity. Their base is combined in the endocast, owing to their shared position within the fossa acustico-facialis at the medial surface of the prootic. The canals of three rami can be discerned, but a single canal for the facial nerve exits into the canalis cavernosus in an anteroventral and lateral direction, and two short, anteroposteriorly aligned canals for the acoustic nerve rami are directed dorsolaterally into the cavum labyrinthicum. The passage of CN VII of *R. pulchriceps* is consistent with the patterns observed in cryptodires, including *T. scripta* (see section 'Brain morphology, cranial nerves and comparisons with the brain cavity in *T. scripta*'), but is distinct from the condition in pleurodires (Gaffney, 1979; Ferreira *et al.*, 2018) and that in some extinct marine turtles, such as plesiochelyids (see discussion by Evers & Benson, 2019: character 127).

The endocast is mediolaterally constricted at the metencephalon, posterior to the position of the fossa acustico-facialis. The vestibular organ (endosseous labyrinth) is positioned at the level of this constriction. The endosseous labyrinth and cranial endocast are confluent via the hiatus acusticus, an unossified space between the medial margins of the prootic and opisthotic. As a result, the separation between the endosseous labyrinth and brain cavity cannot be determined exactly, and the surface of the endocast facing the labyrinth is somewhat arbitrary (see 'Endosseous labyrinth and associated structures' below, for details of how the endosseous labyrinth has been segmented along the hiatus acusticus). In its dorsal part, the endocast space for the inner ear has a short, dorsolaterally directed protuberance, which represents the endolymphatic duct that passes through the supraoccipital dorsolaterally to the common crus.

The ventral surface of the metencephalon is a convex hemisphere that fills the cup-shaped dorsal surface of the parabasisphenoid. At the posterior border of the convex hemisphere, there are two small ventral protuberances to either side of the endocast midline, which are formed by the centrally positioned basis tuberculi basalis on the anterior margin of the basioccipital.

The metencephalon and myelencephalon of the hindbrain form the pontine flexure. In *R. pulchriceps*, the pontine flexure is less marked than the cephalic flexure. The myelencephalon is horizontally oriented posterior to the pontine flexure but continues as a short tubular process posterior to the level of the inner ear. The medulla oblongata is narrower and lower than the metencephalon region of the hindbrain and does not expand toward the foramen magnum. Ventrally, the surface of the myelencephalon is smooth, because a crista dorsalis basioccipitalis is absent in CAMSM B55775 (but present in some other specimens of *R. pulchriceps*; see Evers *et al.*, 2019).

The glossopharyngeal nerve (CN IX) is associated with three foramina in *R. pulchriceps*: the medial foramen for the exit of the nerve from the brain, the internal foramen on the ventral surface of the cavum labyrinthicum at the base of the processus interfenestralis, and the external foramen entering the recessus scalae tympani. The course of the nerve between the medial foramen and the short canal spanning the internal and external foramina has been segmented continuously on the floor of the cavum labyrinthicum, which is in accordance with our observations on the path of this nerve in *T. scripta* (see section 'Brain morphology, cranial nerves and comparisons with the brain cavity in *T. scripta*'). Consequently, CN IX is visible as a long, thin structure diverging laterally from the endocast and extending through parts of the labyrinth model (see Fig. 3C). Directly posterior to the internal glossopharyngeal (CN IX) foramen is the anterior jugular foramen, through which several structures pass, including the vagus (CN X) and accessory (CN XI) nerves. This entire foramen has been segmented as a single structure, meaning that it is shown as a narrow, dorsoventrally high volume. Immediately anterior to the foramen magnum, the hypoglossal nerve (CN XII) rami diverge ventrolaterally from the endocast, exiting through two anteroposteriorly aligned foramina.

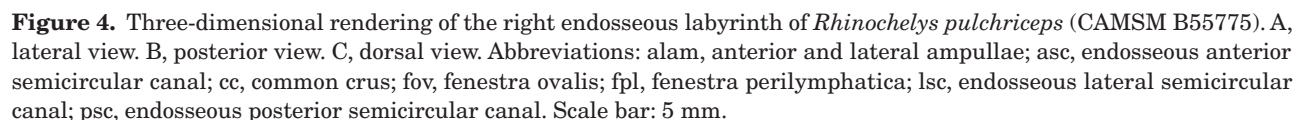
Endosseous labyrinth and associated structures

Morphological information on the inner ear of turtles has been limited to a few studies based on anatomical dissections, naturally preserved fossil endocasts, or digital renderings of the endocast in extant and extinct species based on μ CT data (Zangerl, 1960; Gaffney & Zangerl, 1968; Baird, 1974; Gaffney, 1977, 1982; Georgi, 2008; Thewissen & Nummela, 2008; Walsh *et al.*, 2009; Carabajal *et al.*, 2013, 2017; Neenan *et al.*, 2017; Ferreira *et al.*, 2018; Lautenschlager *et al.*, 2018).

The inner ear of vertebrates is organized roughly into a superior division (semicircular canals and ampullae) and an inferior division (sacculae and cochlea) (Wever, 1978; Georgi & Sipla, 2008). The

In turtles, the auditory part of the inner ear and the vestibule are not completely enclosed by bone, making segmentation difficult. Medially, the endosseous labyrinth is confluent with the brain cavity via the

In the endosseous labyrinth of *R. pulchriceps*, the three semicircular canals can be distinguished clearly (Fig. 4). Anterior and posterior semicircular canals meet within the supraoccipital, forming the common crus. From the common crus, the anterior semicircular canal extends anterodorsolaterally within the supraoccipital, then turns in an anteroventral and lateral direction to pass through the prootic. The part of the anterior semicircular canal housed within the prootic is very weakly arched, and the greatest curvature is accommodated between the dorsal end of the prootic and the common crus. In anteroventral and lateral directions, the anterior semicircular canal terminates in the anterior ampulla. The anterior ampulla of *R. pulchriceps* is confluent with the lateral ampulla, which is situated at the anterior end of the lateral semicircular canal. In *R. pulchriceps*, the combined anterior and lateral ampullae form a slightly dorsally convex and roughly oval surface between the anterior and lateral semicircular canals and the ventral base of the common crus. The utricle,



which connects the common crus with the ampullae, is not discernible as a distinct canal, but is merged with the dorsal part of the central cavity of the vestibular endocast.

The posterior semicircular canal is roughly symmetrical to the anterior semicircular canal (Fig. 4A). Analogously to the anterior semicircular canal, the posterior semicircular canal extends in a posterodorsal and lateral direction from the common crus into the posterodorsal part the supraoccipital, then turns in a posteroventral and lateral direction through the opisthotic. The opisthotic part of the posterior semicircular canal is also almost straight, with the greatest curvature of the canal again being between the dorsal end of the opisthotic and the common crus. According to Wever (1978), the membranous posterior semicircular duct of reptiles continues ventrally to the posterior extent of the membranous lateral semicircular duct and turns in an anteroventral and medial direction to join the common crus ventrally. We confirm that this configuration is present in extant turtles based on our scan data of *T. scripta* (see section 'Endosseous and membranous labyrinth geometry of *T. scripta*'). However, the endosseous labyrinth of *R. pulchriceps* (and other turtles; S.W.E., pers. obs.) does not mirror this portion of the semicircular duct morphology; the ventral path of the posterior semicircular canal cannot be distinguished from the posteromedial course of the lateral semicircular canal, as these structures traverse a joint cavity within the ventromedial part of the opisthotic part of the endosseous labyrinth, which is further confluent anteriorly with the saccule. Therefore, the ventrolateral part of the posterior semicircular canal and the posterior part of the lateral semicircular canal are merged into a large cavity that represents the posterolateral-most corner of the inner ear model presented here.

The common crus is strongly concave between the highest extent of the anterior and posterior semicircular canals, a feature that is observed in many, but not all, turtles (S.W.E., pers. obs.). The functionality and distribution of this feature among turtles are not understood. The common crus of *R. pulchriceps* is short and has a diameter about twice as wide as that of the anterior and posterior semicircular canals, which assume a subequal diameter and approximately circular cross-section. Measuring the divergence angle between the anterior and posterior semicircular canals was difficult, because the canals are not perfectly straight. Here, we projected a vertical plane through the centre of the straight parts of the anterior and posterior semicircular canals (i.e. the parts from the ampullae to the dorsal-most points of the respective canals) and measured the angle between these planes. The divergence angle was 79° and can be approximated from Figure 4C. Although almost symmetrical, there

are some minor differences between the anterior and posterior semicircular canals. The anterior canal is slightly longer than its posterior counterpart, and the posterior canal is slightly more strongly directed laterally than the anterior semicircular canal; if a coronal plane is laid through the midpoint of the common crus, the anterior semicircular canal accounts for the greater portion of the total divergence angle between both canals. The dorsal-most point of the anterior semicircular canal also extends slightly more dorsally than the corresponding point on the posterior semicircular canal.

The lateral semicircular canal appears to be the shortest in the digital models. This is because its posteromedial path, medial to the posterior semicircular canal, is obscured by the fact that it is housed in a single space together with the ventromedial path of the posterior semicircular canal. Therefore, the course of the lateral semicircular canal can be traced only from the lateral ampulla to the posterior-most corner of the labyrinth. Between these points, the lateral semicircular canal is laterally arched, meaning that it has a convex lateral outline in dorsal view. The curvature of the lateral semicircular canal is stronger than that of the other semicircular canals. The cross-section of the lateral semicircular canal is elliptical (which is also the case in *T. scripta*; see section 'Endosseous and membranous labyrinth geometry of *T. scripta*'), because it is dorsoventrally thin and mediolaterally broad. The medial margin of the lateral semicircular canal is separated from the saccule by a bar formed by the opisthotic. In the model, this feature shows as a vertically directed opening between the lateral semicircular canal and the central area of the vestibular endocast. The lateral canal is not parallel to the skull roof (as formed by the parietals) or the palate (as formed by the pterygoids), which form two parallel horizontal planes. Instead, the lateral canal intersects an axial plane parallel to the parietals/pterygoid at ~15°, whereby the anterior portion of the canal is dorsally inclined in relationship to the horizontal plane defined by the skull roof and palate.

The turtle auditory system has several specializations that are not found in other reptiles. The turtle inner ear lacks the round window (fenestra rotunda) that serves as a pressure-relief structure in other reptilian inner ears, but instead has a continuous, re-entrant fluid-flow system around the stapedial footplate in a space named the pericapsular recess (Henson, 1974; Wever, 1978; Hetherington, 2008). The pericapsular recess is not formed by bone, because it fills parts of the recessus scalae tympani and the cavum acustico-jugulare, and thus cannot be reconstructed for *Rhinochelys*. However, the pericapsular sac is situated in the recessus scalae tympani and communicates with the endosseous labyrinth through the fenestra

perilymphatica, a ventrally open aperture on the medial margin of the processus interfenestralis. The fenestra perilymphatica in *R. pulchriceps* is posteroventrally directed and subcircular in outline (Fig. 4B). The pericapsular recess in *R. pulchriceps* would have extended from the recessus scalae tympani into the anteromedial section of the cranioquadrate space portion of the cavum acustico-jugulare, lateral to the fenestra ovalis, which is covered by the pericapsular recess.

Another feature of the turtle auditory system is a medially constricted middle ear, formed largely by the quadrate, which has a tubular recess or stapedial foramen that funnels the stapes medially (Henson, 1974). This has been interpreted as an aquatic adaptation in turtles in general (Christensen-Dalsgaard *et al.* 2012), because the closed middle ear region consists of cancellous bone that might isolate the inner ear acoustically to prevent bone conduction of sound waves under water, making the tympanic middle ear with the ossicular chain the only relevant structure for sound reception in turtles

and permitting directional hearing when submerged (Hetherington, 2008). However, μ CT scans of *R. pulchriceps* show that bones that do not contribute to the otic capsule, such as the parabasisphenoid, are cancellous to the same extent as the otic capsule. Also, large parts of the inner ear are surrounded by open spaces, including the widely open sutural contacts between the prootic, opisthotic and supraoccipital; therefore, acoustic isolation by cancellous bone does not seem likely.

NEUROANATOMY OF THE EXTANT TURTLE *T. SCRIPTA*

Brain morphology, cranial nerves and comparisons with the brain cavity in T. scripta

The endocast of the brain cavity of *T. scripta* is similar to those described for other extant turtles (Lautenschlager *et al.*, 2018) and fossil turtles, such as that of *R. pulchriceps* described herein. It is tubular, with weak cephalic and pontine flexures, has a low dural peak and relatively smooth external surfaces without clear demarcations for the cerebral

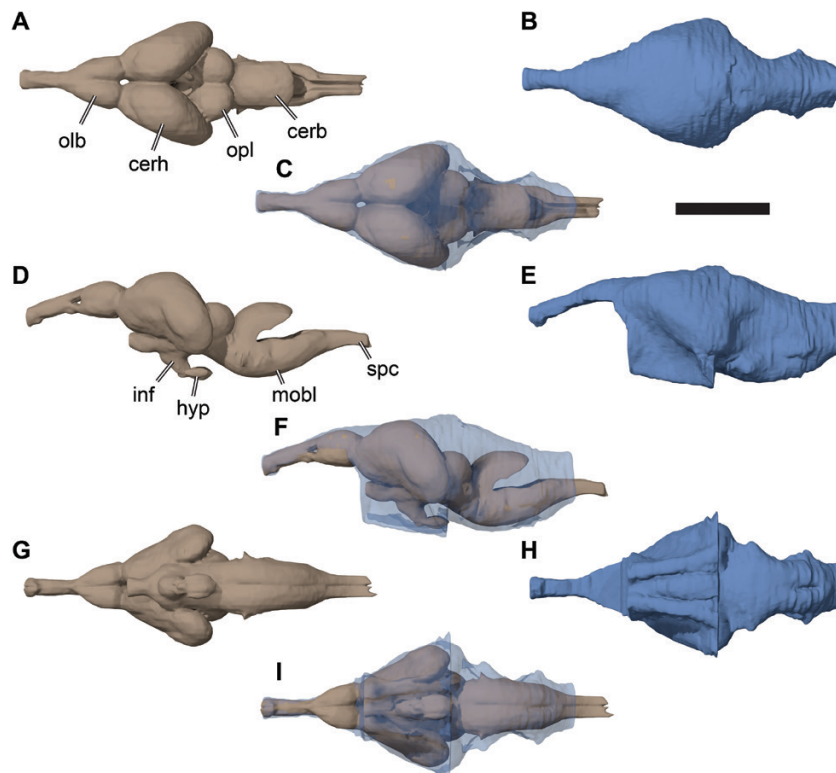


Figure 5. Three-dimensional renderings of the brain and endocast of the brain cavity of *Trachemys scripta*. A, D, G, brain. B, E, H, endocast of the brain cavity. C, F, I, endocast of the brain cavity rendered transparent, with solid model of brain inside. A–C are in dorsal view, D–F in left lateral view and G–I in ventral view. Abbreviations: cerb, cerebellum; cerh, cerebral hemisphere; hyp, hypophysis; inf, infundibulum; mobl, medulla oblongata; olb, olfactory bulb; opl, optic lobe; spc, spinal cord. Scale bar: 10 mm.

hemispheres or optic lobes (Fig. 5B, E). The endocast of the sella turcica forms a ventrally placed median expansion for the pituitary in *T. scripta* (Fig. 5E, H), which is also the case in *R. pulchriceps*.

Given that the main goal of this study is not a comprehensive description of the brain of *T. scripta*, we provide only brief comments here on the shape and identity of structures. The brain of *T. scripta* has

the same general features reported for other reptilian brains, particularly with regard to the relative sizes of brain tissues such as the cerebral hemispheres, optic lobes and cerebellum (Kardong, 2008). The olfactory bulbs of *T. scripta* are ovoid hemispheres at the anterior end of the brain and are much closer to the cerebral hemispheres than reported for crocodiles (Kardong, 2008). Left and right olfactory bulbs of *T. scripta* are

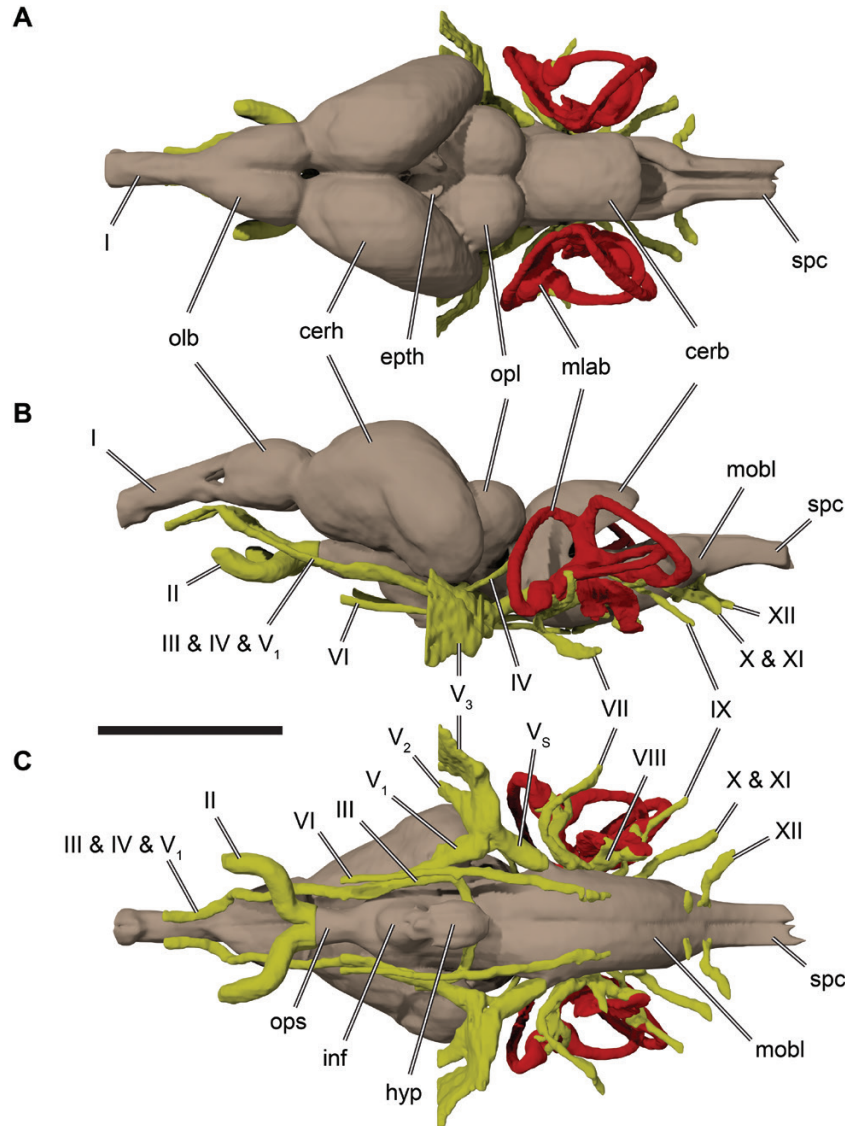


Figure 6. Three-dimensional rendering of the brain, membranous labyrinths and cranial nerves of *Trachemys scripta*. A, dorsal view. B, left lateral view. C, ventral view. Abbreviations: cerb, cerebellum; cerh, cerebral hemisphere; eph, epithalamus; hyp, hypophysis; I, olfactory nerve (cranial nerve I); II, optic nerve (cranial nerve II); III, oculomotor nerve (cranial nerve III); inf, infundibulum; IV, trochlear nerve (cranial nerve IV); IX, glossopharyngeal nerve (cranial nerve IX); mlab, membranous labyrinth; mobl, medulla oblongata; olb, olfactory bulb; opl, optic lobe; ops, optic stalk; spc, spinal cord; V1, ophthalmic branch of trigeminal nerve (cranial nerve V1); V2, maxillary branch of trigeminal nerve (cranial nerve V2); V3, mandibular branch of trigeminal nerve (cranial nerve V3); VI, abducens nerve (cranial nerve VI); VII, facial nerve (cranial nerve VII); VIII, vestibulocochlear (= statoacustico) nerve (cranial nerve VIII); X, vagus nerve (cranial nerve X); XI, accessory nerve (cranial nerve XI); XII, hypoglossal nerve (cranial nerve XII). Scale bar: 10 mm.

separated across the midline by a moderately deep dorsal sulcus (Fig. 6A). Anteriorly, the olfactory bulbs become smaller and send off the olfactory nerve (CN I) anteriorly. The olfactory bulbs of *T. scripta* are notably larger than those described for *Dermochelys coriacea* (Wyneken, 2001). The contact between the olfactory bulbs and the posteriorly adjacent cerebral hemispheres is constricted to all sides, meaning that both structures are clearly separated from one another (Fig. 6). The cerebral hemispheres form large ovoid expansions to either side of the midline. Anteriorly, right and left hemispheres are positioned close to the midline, where they are separated by a deep sulcus anteriorly. The posteroventral parts of the cerebral hemispheres diverge away from the midline (Fig. 6A). The cerebral hemispheres are more prominent than in *Dermochelys coriacea*, but notably smaller than in *Alligator mississippiensis* (Daudin, 1802) (Kardong, 2008). The posterior surfaces of the cerebral hemispheres of *T. scripta* slope steeply ventrally, creating a cephalic flexure that is much more pronounced than in the endocast of the brain cavity (Fig. 6B). The diencephalon is positioned posteriorly between the laterally diverging cerebral hemispheres, and some features are visible on its dorsal surface. Most conspicuous are paired small dorsal projections to either side of the midline, which are anterolaterally connected to the cerebral hemispheres and continue for a short distance posteromedially (Fig. 6A). However, they disappear before reaching either the midline medially or the optic lobes posteriorly. We identify these structures as the epithalamus. The pineal gland arises centrally between these epithalamus structures, but has not been segmented because the pineal tissue did not show clearly in our μ MRI data. However, the pineal gland tissue extends dorsal to the dural peak seen in the brain cavity endocasts (Fig. 5E).

Two main structures are apparent on the anteroventral side of the forebrain: the optic stalk as a large anterior projection, which then gives off the paired optic nerve (CN II; Fig. 6C); and the posteroventrally curved infundibulum, leading to the hypophysis (= pituitary gland; Fig. 6C).

The midbrain region is dominated by two hemispherical optic lobes, which are posteriorly positioned between the posteroventrally and laterally diverging cerebral hemispheres (Fig. 6A, B).

Posterior to the optic lobes, the cerebellum forms a posterodorsally arched projection, which has an anteroposteriorly convex dorsal surface (Fig. 6A, B). The dorsal surface of the cerebellum is also convex mediolaterally and not incised by a median sulcus. The ventral surface of the hindbrain forms a ventrally convex, wide arc, and the medulla oblongata becomes more slender posteriorly, continuous with the spinal cord.

The cranial nerve pattern of *T. scripta* is generally similar to that inferred for osteological specimens of turtles by reference to the cranial nerve foramina, such as in *R. pulchriceps* (see section 'Cranial endocast'). However, additional details and nerves that do not leave osteological correlates are also observable in our data of *T. scripta*. The olfactory nerve (CN I) of *T. scripta* appears in the scans as a large bundle of nervous tissue that lies in the sulcus olfactorius. It fills the entire structure, meaning that reconstructed endocasts of the sulcus olfactorius, or the olfactory canal as present in *R. pulchriceps*, form a reasonably accurate representation of the original nervous tissue.

The optic nerve (CN II) does not leave an osteological trace in turtles, and thus could not be reconstructed in *R. pulchriceps* (see section 'Cranial endocast'), but the paired optic nerves of *T. scripta* are extremely thick, diverge with a sharp lateral turn from one another after leaving the optic stalk and continue anteriorly to innervate the medial surface of each eyeball (Fig. 6C).

The oculomotor nerve (CN III) also leaves no osteological trace and has thus not been reconstructed for *R. pulchriceps*. In *T. scripta*, CN III begins fairly close to the midline, at the ventral surface of the brain at the interface of the mid- and hindbrain. Right and left CN III take sharp lateral turns after emerging from the brain (Fig. 6C) and then continue anteriorly, together with the ophthalmic branch of the trigeminal nerve (CN V₁) and the CN IV, towards the eyes (Fig. 6B, C).

The trochlear nerve (CN IV) of *T. scripta* originates relatively high dorsally on the lateral surface of the brain, in the constriction that marks the border between the optic lobe and the cerebellum (Fig. 6B). It extends anteroventrally and joins the course of CN III and CN V₁. Again, this nerve leaves no osteological trace.

The trigeminal nerve (CN V) of *T. scripta* emerges as a thick stalk from the lateral brain surface (Fig. 6C), continues anterolaterally and slightly ventrally and enters the cavum epiptericum via the 'internal' trigeminal foramen (see discussion on trigeminal foramen nomenclature below), which is formed as a dorsally open notch between each clinoid process of the parabasisphenoid and the prootic. Within the cavum epiptericum, it expands into its ganglion, which is visible in the slice data as a large mass of nervous tissue. We segmented the three main branches of the trigeminal nerve. The ophthalmic branch of the trigeminal nerve (CN V₁) is anteriorly directed from the trigeminal ganglion (Fig. 6C) and continues at the external surface of the cartilage lining the brain case anteriorly towards the eyes. The maxillary (CN V₂) and mandibular (CN V₃) branches of the trigeminal nerve separate within the cavum epiptericum, but close to the 'external' trigeminal foramen, through which they exit into the adductor chamber. Both nerve branches

are surrounded by adductor musculature, and CN V₂ turns anteriorly upon exiting the 'external' trigeminal foramen (Fig. 6C). Cranial nerve V₃ is the largest of the three trigeminal branches in *T. scripta* and forms a broad, sheet-like nervous arrangement interbedded between musculature (Fig. 6B, C). It extends laterally and, ultimately, ventrally.

The abducens nerve (CN VI) of *T. scripta* is visible as an anteroposteriorly long, nearly straight structure at the ventral surface of the brain (Fig. 6C). It exits the brain tissue in the form of several thin strands that anastomose to a more compact nerve bundle that extends along the dorsal surface of the parabasisphenoid before entering that bone and extending anteriorly through it. The foramina for CN VI are often observed in the parabasisphenoids of turtles (e.g. Gaffney, 1979), although they are not always visible in CT scans of fossils owing to their small size (see *R. pulchriceps* description, above).

The facial nerve (CN VII) emerges together with the vestibulocochlear (= statoacustico) nerve (CN VIII) from the lateral surface of the hindbrain of *T. scripta*, in a position approximately halfway along the anteroposterior length of the cerebellum (Fig. 6C). Cranial nerve VII forms a semicircular, anteriorly convex arc (Fig. 6B, C). This nerve can also be followed for a comparatively long distance in fossils or dry specimens, because it traverses the prootic bone (e.g. Gaffney, 1979). Cranial nerve VIII of *T. scripta* is described in greater detail in the subsection 'Innervation of the membranous labyrinth in *T. scripta*' owing to its innervation of the inner ear.

The glossopharyngeal nerve (CN IX) starts at the same dorsoventral level as CNs VII and VIII, but is positioned slightly posteriorly to the latter (Fig. 6B, C). The CN IX of *T. scripta* has a posterolateral course and traverses through parts of the opisthotic (e.g. Gaffney, 1979), as also evident from our scans of *R. pulchriceps*.

The vagus nerve (CN X) and accessory nerve (CN XI) of *T. scripta* were not distinguishable as separate structures and have been segmented as a single model (Fig. 6B, C). They emerge from the lateral surface of the hindbrain, somewhat posteroventrally to CN IX, and extend through the recessus scalae tympani, where they leave no osteological correlate (see *R. pulchriceps* above).

Two short rami of the hypoglossal nerve (CN XII) of *T. scripta* could be identified as exiting the brain ventrolaterally near the position of the foramen magnum (Fig. 6C). The positions of these nerves are usually readily identifiable in fossils and dry specimens by their characteristic foramina in the exoccipital.

Our segmentations of the brain tissue of *T. scripta* show that the brain cavity is an extremely poor predictor of brain tissue volume and shape (Fig. 5). From the brain endocast, only parts of the olfactory

region can be roughly approximated in terms of size and shape.

Endosseous and membranous labyrinth geometry of T. scripta

The geometry of the endosseous semicircular canals is generally assumed to reflect important aspects of the shape of the membranous semicircular ducts, particularly the arc sizes and planar orientations (Spoor & Zonneveld, 1998; Ekdale, 2016). This is despite the fact that the geometry of the endosseous labyrinth does not provide an exact representation of the membranous labyrinth (e.g. Baird, 1970; Spoor & Zonneveld, 1998; Witmer *et al.*, 2008). The relationship between the endosseous and membranous labyrinths has not been considered closely in many cases, and size correlations between endosseous semicircular canals and membranous semicircular ducts have received only generalized quantifications (e.g. Baird, 1970: p. 206, for lizards, 'approximately three-fourths the diameter of the canals they occupy') and vary between animal groups (Wilson & Melville Jones, 1979). Our comparative dataset of endosseous labyrinths from extant and extinct turtles shows great variability in endosseous canal diameters. This raises the question of whether, and which, parts of the membranous labyrinth morphology can be inferred from endocasts of the endosseous structure. We use models of *T. scripta* to assess the accuracy with which the digital endocasts of the osteological correlates for the sensory structures (i.e. the endocasts of the endosseous labyrinth) reflect the shape of the real organs (i.e. membranous labyrinth). Such assessments are important to validate quantitative analyses of digital endocasts and to enable comparisons of higher taxa with different endosseous endocasts of the labyrinth organ.

As we show in this section, most aspects of endosseous labyrinth morphology in *T. scripta* are consistent with those of other turtles, including stem turtles (see Lautenschlager *et al.*, 2018). Additionally, the membranous labyrinth morphology is consistent with that of other reptiles, including birds. Therefore, and despite only providing information on a single turtle taxon, we interpret our data to indicate that turtles conform to a generalized reptilian membranous labyrinth morphology (e.g. Wever, 1978).

The most important observations from our membranous and endosseous labyrinth comparisons can be summarized as follows: (1) the membranous labyrinth of *T. scripta* conforms to the pattern of semicircular canal geometry of other reptiles, including birds (e.g. Wever, 1978); (2) the endosseous semicircular canals are much larger in cross-sectional area than their respective membranous ducts (see quantification, below); (3) identifiable endosseous

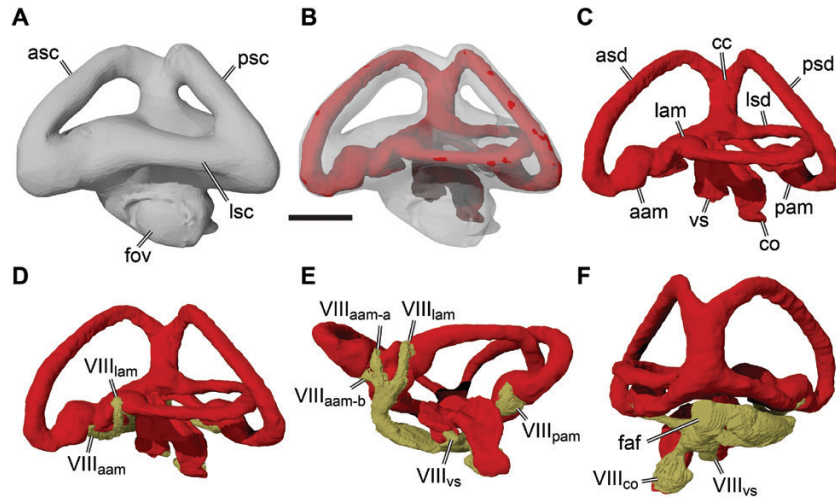


Figure 7. Endosseous and membranous labyrinth morphology and innervation of *Trachemys scripta* illustrated by three-dimensional renderings of the left labyrinth and associated acoustic nerves. A, lateral view of endosseous labyrinth. B, lateral view of endosseous labyrinth rendered transparent, showing membranous labyrinth inside. C, lateral view of membranous labyrinth. D, lateral view of membranous labyrinth and innervation. E, ventral view of membranous labyrinth and innervation. F, posterior view of membranous labyrinth and innervation. Abbreviations: aam, anterior ampulla; asc, endosseous anterior semicircular canal; asd, membranous anterior semicircular duct; cc, common crus; co, cochlea; faf, fossa acustico-facialis; fov, fenestra ovalis; lam, lateral ampulla; lsc, endosseous lateral semicircular canal; lsd, membranous lateral semicircular duct; pam, posterior ampulla; psc, endosseous posterior semicircular canal; psd, membranous posterior semicircular duct; vs, vestibule; VIII, acoustic nerve (cranial nerve VIII); VIIlaam, anterior ampulla branch of the acoustic nerve; VIIlaam-a, sub-branch a of anterior ampulla branch of the acoustic nerve; VIIlaam-b, sub-branch b of anterior ampulla branch of the acoustic nerve; VIIlco, cochlear branch of the acoustic nerve; VIIllam, lateral ampulla branch of the acoustic nerve; VIIlpam, posterior ampulla branch of the acoustic nerve; VIIlvs, vestibular branch of the acoustic nerve. Scale bar: 2 mm.

posterior and lateral canals reflect only the partial courses of the respective membranous ducts; and (4) the endosseous anterior semicircular canal provides the most accurate reflection of the membranous duct out of the three semicircular canals.

In *T. scripta*, the membranous anterior semicircular duct traverses through the endosseous anterior semicircular canal (Fig. 7). Anteroventrally, the canal meets the anterior ampulla, and the intersection of these two structures is clearly marked in the membranous labyrinth by a sudden expansion of the membranous tissue. In the endosseous labyrinth, the region around the anterior ampulla is also expanded, but the transition from canal to ampulla is more gradual. Dorsomedially, the anterior membranous ducts and corresponding endosseous canals curve to form a wide arc before they meet the posterior semicircular canal in the common crus. Despite difficulties in discerning the point of transition between the anterior semicircular canal and ampulla in the endosseous labyrinth, the endosseous anterior semicircular canal represents the length of the membranous anterior semicircular duct adequately in *T. scripta*.

The membranous posterior semicircular duct of *T. scripta* passes from the common crus posteriorly

through the endosseous posterior semicircular canal (Fig. 7). In the membranous labyrinth, the ventral part of the posterior semicircular duct extends ventrally to the posterior half of the lateral semicircular duct, without contacting the latter. It then extends medially for a short distance and merges with the thickened posterior ampulla. Neither the posterior ampulla nor the ventromedial course of the posterior duct is evident from the endocast of the endosseous labyrinth in *T. scripta* (and other turtle endosseous labyrinth endocasts), because this portion of the endosseous labyrinth also houses parts of the membranous lateral semicircular canal. The endosseous posterior semicircular canal is therefore shorter than the membranous duct. The same pattern of partly confluent posterior and lateral endosseous semicircular canals is seen in crocodiles and rhynchocephalians (Walsh *et al.*, 2009) and in some mammals, in which this is inferred to be the ancestral condition based on fossils of Mesozoic metatherians and eutherians (Ekdale, 2016). In mammals, this feature is referred to as a 'secondary common crus' (Ekdale, 2016). Digital reconstructions based on histological serial sections show that the membranous semicircular ducts remain separate

from one another within the secondary common crus of the mammal *Ornithorhynchus anatinus* (Shaw, 1799) (duck-billed platypus; [Schultz et al., 2017](#)). Given that the spatial relationships of the lateral and posterior semicircular ducts within a single osseous cavity are the same in *T. scripta*, we adopt the term 'secondary common crus' here. A secondary common crus is not universally present in reptiles; in birds ([Benson et al., 2017](#)) and in some squamates ([Walsh et al., 2009](#); [Yi & Norell, 2015](#)), the ventromedial part of the endosseous posterior semicircular canal curves around the posterior portion of the endosseous lateral semicircular canal. Thus, in these taxa, both endosseous canals are separate structures along their entire course, and therefore more adequately reflect membranous labyrinth morphology than is the case in turtles or other animals with a secondary common crus. However, the observation that reptiles with a secondary common crus, such as *T. scripta*, retain separate posterior and lateral semicircular ducts within the secondary common crus indicates that the relative positions and geometrical relationships of the semicircular ducts are identical to those reptiles that lack a secondary common crus, such as birds. This is despite other shape differences seen between turtles and birds, such as the extreme roundness of canal arcs in birds (e.g. [Benson et al., 2017](#)) in comparison with relatively straight canal arcs in turtles.

The mediodorsal part of the posterior semicircular canal is visible in the endocasts of the endosseous labyrinth in *T. scripta*. The endosseous posterior semicircular canal forms an arc that extends from the posterolateral margin of the vestibular endocasts to the common crus. The arc of the posterior semicircular duct is relatively smaller than the anterior duct, but it is not much shorter as is the case in birds (e.g. [Walsh et al., 2009](#): fig. 1; [Benson et al., 2017](#)), pterosaurs ([Witmer et al., 2003](#); [Codorníu et al., 2016](#)) or some non-avian dinosaurs (e.g. [Martínez et al., 2016](#)). The relatively weak asymmetry of anterior and posterior canals is comparable to that of crocodiles, phytosaurs, rhynchocephalians, sauropterygians and squamates ([Walsh et al., 2009](#): fig. 1; [Yi & Norell, 2015](#); [Lautenschlager & Butler, 2016](#); [Neenan et al., 2017](#)).

The lateral semicircular canal and duct of *T. scripta* begins anteriorly in the lateral ampulla and extends as an arc posterolaterally ([Fig. 7](#)). The position of the lateral ampulla is evident from the endosseous labyrinth endocast as a low and broad expansion but, similar to the condition in the anterior semicircular canal, the intersection of ampulla and canal is much weaker in the endosseous endocast than in the soft tissue model. The membranous lateral semicircular duct passes towards the common crus along a wide arch, but anteromedially with respect to the membranous posterior semicircular canal, meaning that both

structures are separate. All parts of the membranous lateral semicircular duct are aligned on a horizontal plane, meaning that the medial end of the duct merges with the common crus on the same horizontal level as the lateral ampulla. As mentioned above, the posteromedial course of the lateral semicircular duct is not visible in the endosseous labyrinth model. This part is instead integrated in a large cavity, the secondary common crus, which houses the centrally positioned vestibular part of the labyrinth and the ventromedial part of the posterior duct.

The endosseous semicircular canals are much larger in cross-sectional diameter than their respective membranous ducts. However, all semicircular canals and ducts retain approximately the same diameters throughout most of their courses, except for portions of the endosseous canals close to the position of the ampullae. We measured the semicircular canal and duct diameters and cross-sectional areas to quantify and compare the canal and duct thickness. Volumetric comparisons are potentially misleading, owing to the incorporation of the inferior division of the labyrinths in our models. Given that neither the semicircular ducts nor the semicircular canals seem to vary much in diameter throughout most of their lengths, we measured the diameters and areas for each duct and canal on a single slice positioned approximately at mid-length of each semicircular canal. To produce an accurate cross-sectional measurement, we chose a CT slice in which the respective canal/duct traverses two of the three orientation planes used in CT-segmentation software (i.e. coronal, axial, sagittal) perpendicularly and is parallel to the third. To achieve cross-sections that were orthogonal to one of the orientation planes for the anterior and posterior semicircular canals (which traverse the orientation planes obliquely in regularly oriented specimens), we re-sliced the MIMICS projects and manually re-orientated the canals. We measured the minimal and maximal diameters and areas of the membranous semicircular ducts and the endosseous semicircular canals using the 'Ellipse' measurement tool in MIMICS v.18.0.

Measurements for *T. scripta* are shown in [Table 1](#). The semicircular ducts are almost perfectly circular in cross-section [see [Table 1](#); e.g. minimal diameter for the lateral semicircular duct is $d(\text{duct})_{\min} = 0.45$ mm; maximal diameter of $d(\text{duct})_{\max} = 0.48$ mm]. The endosseous semicircular canals are much larger and deviate much more strongly from a circular shape [see [Table 1](#); e.g. the minimal diameter for the lateral semicircular canal is $d(\text{canal})_{\min} = 1.08$ mm, and the maximal diameter is $d(\text{canal})_{\max} = 1.39$ mm]. As a result, the cross-sectional areas of the membranous lateral semicircular ducts fill only between 14.4 (lateral) and 26.0% (anterior) of the cross-sectional areas of the endosseous semicircular canals (see [Table 1](#)).

Table 1. Semicircular canal and duct measurements for *Trachemys scripta* and *Rhinochelys pulchriiceps*

Measurement	<i>Trachemys scripta</i>	<i>Rhinochelys pulchriiceps</i>
Anterior semicircular duct		
Length (mm)	9.59	—
Minimal diameter (mm)	0.49	—
Maximal diameter (mm)	0.50	—
Cross-sectional area (mm ²)	0.19	—
Percentage of ASC diameter	26.0	—
Anterior semicircular canal		
Length (mm)	7.49	9.96
Minimal diameter (mm)	0.86	1.23
Maximal diameter (mm)	1.08	1.46
Cross-sectional area (mm ²)	0.73	1.42
Diameter–arc length ratio	0.13	0.18
Posterior semicircular duct		
Length (mm)	9.84	—
Minimal diameter (mm)	0.44	—
Maximal diameter (mm)	0.47	—
Cross-sectional area (mm ²)	0.16	—
Percentage of PSC diameter	17.0	—
Posterior semicircular canal		
Length (mm)	7.17	8.56
Minimal diameter (mm)	1.09	1.18
Maximal diameter (mm)	1.11	1.53
Cross-sectional area (mm ²)	0.94	1.42
Diameter–arc length ratio	0.15	0.16
Lateral semicircular duct		
Length (mm)	10.00	—
Minimal diameter (mm)	0.45	—
Maximal diameter (mm)	0.48	—
Cross-sectional area (mm ²)	0.17	—
Percentage of LSC diameter	14.4	—
Lateral semicircular canal		
Length (mm)	3.43	3.68
Minimal diameter (mm)	1.08	1.37
Maximal diameter (mm)	1.39	2.07
Cross-sectional area (mm ²)	1.18	2.23
Diameter–arc length ratio	0.36	0.47

Abbreviations: asc, endosseous anterior semicircular canal; lsc, endosseous lateral semicircular canal; psc, endosseous posterior semicircular canal.

Innervation of the membranous labyrinth in *T. scripta*

Our μ MRI data of *T. scripta* were well enough resolved to segment the detailed innervation of the vestibular organ (Fig. 7). The divisions and innervations of branches observed here are consistent with other descriptions of tetrapod vestibulocochlear anatomy (e.g. Retzius, 1884; Baird, 1970; Wever, 1978). The

vestibulocochlear (= statoacustico) nerve (CN VIII) of *T. scripta* begins medially in the fossa acustico-facialis, which is positioned slightly ventrally to the level of the lateral semicircular duct, but otherwise in a central position medial to the membranous labyrinth (Fig. 7F). Immediately after entering the cavum labyrinthicum, CN VIII splits into two large branches. The anterior of the two branches extends towards the junction of the anterior and lateral ampullae and splits ventrally to these structures into three short subordinate branches (Fig. 7E). Two of these branches innervate the anterior ampulla, whereby one extends laterally (VIII_{aam-a}) and the other medially (VIII_{aam-b}) around the base of the ampulla. Another small ramus of the anterior branch of CN VIII innervates the lateral side of the lateral ampulla (VIII_{lam}). The second branch of CN VIII extends posteroventrally from the fossa acustico-facialis for a short distance, then splits into three subordinate branches (Fig. 7E, F). The anteriormost of these branches innervates the ventral surface of the vestibule (VIII_{vs}), the central branch attaches to the ventral tip of the cochlea (VIII_{co}), and the posteriormost and longest branch extends to the ventral surface of the posterior ampulla (VIII_{pam}). Here, this branch splits again into an anterior and posterior ramus, which wrap around the ventral side of the posterior ampulla.

DISCUSSION

MARINE ADAPTATIONS IN THE LABYRINTH OF *R. PULCHRICEPS*?

The labyrinth endocast of *R. pulchriiceps* has relatively thick endosseous semicircular canals (i.e. large canal diameters), with relatively high diameter–arc length ratios (see Table 1), when compared qualitatively with those of published terrestrial (Carabajal *et al.*, 2017; Lautenschlager *et al.*, 2018) and non-marine aquatic turtles (Walsh *et al.*, 2009; Neenan *et al.*, 2017; Ferreira *et al.*, 2018; Lautenschlager *et al.*, 2018; present study). This is particularly evident from comparisons with pleurodires, trionychians and chelydroids (see Fig. 8). However, calculated diameter–arc length ratios for the endosseous semicircular canals do not differ greatly between *R. pulchriiceps* and *T. scripta*, although the former does have higher values for all three canals (Table 1). Thick endosseous semicircular canals are also present in fossil (e.g. *Argillochelys cuneiceps* (Owen, 1849) [NHMUK PV R38955, published as *Puppigerus camperi* (Gray, 1831)], Neenan *et al.*, 2017; see Fig. 8) and extant (*L. olivacea*, Neenan *et al.*, 2017; see Fig. 8; *Chelonia mydas* Linnaeus, 1758, Lautenschlager *et al.*, 2018) chelonoids. *Dermochelys coriacea*, the extant leatherback turtle, has extremely thick endosseous semicircular canals (UMZC R3031; Fig. 8).

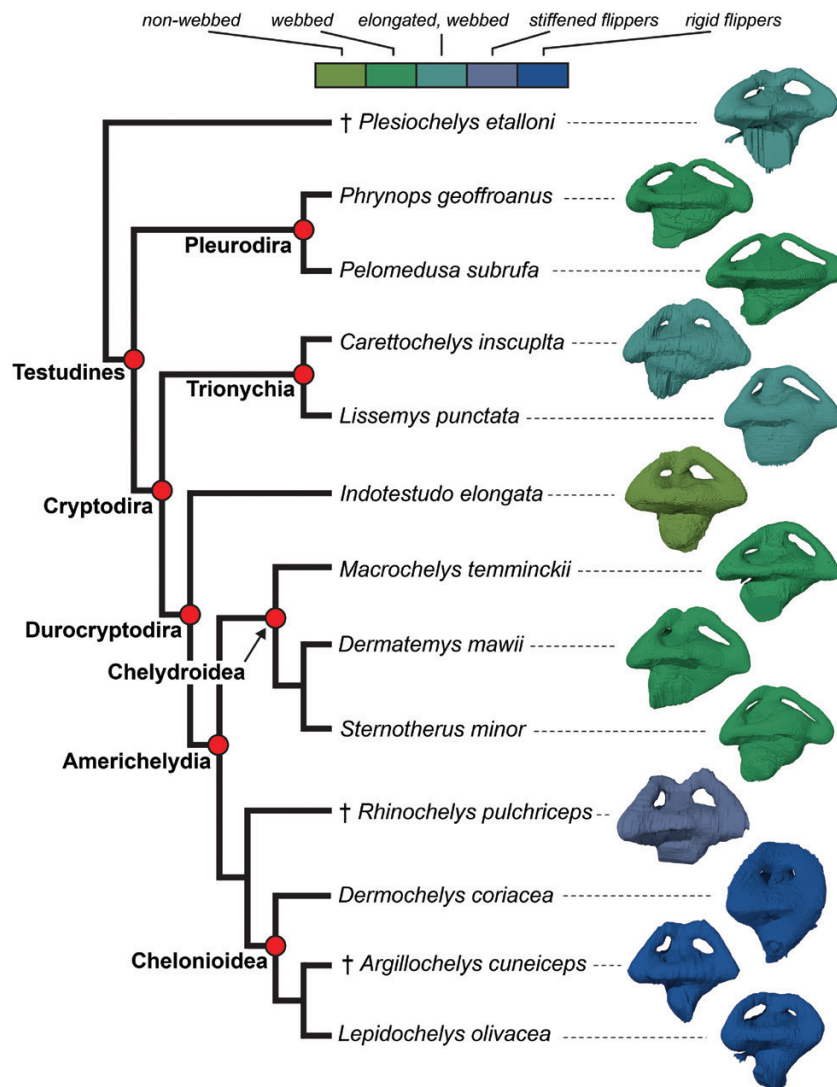


Figure 8. Comparative endosseous labyrinth morphology of selected turtles in their phylogenetic context. The topology follows Evers *et al.* (2019). The colour legend indicates modifications of the hands that are indicative of locomotion type and habitat ecology, with increased aquatic adaptations to the right of the legend. Internal node labels indicate crown groups. Note that the secondarily marine extinct turtle *Plesiochelys etalloni* and trionychians share elongated hands and webbing (assumed for *Plesiochelys etalloni*), but that stiffened flippers occur only in the total group of Chelonioida. Daggers indicate extinct taxa.

Georgi & Sipla (2008) hypothesized that marine animals that are exposed to strong externally forced body rotations (such as surf for juvenile sea turtles) would be expected to show increased sensitivity of the semicircular duct system. Such increases in sensitivity could be achieved by increases in semicircular duct cross-sectional area (Georgi & Sipla, 2008). If endosseous semicircular canal thickness were to scale positively with semicircular duct diameter, the thick canals of chelonioids could be interpreted to confirm the hypothesis of Georgi & Sipla (2008). These features are potentially testable by examining the semicircular ducts

of extant chelonioids. Alternatively, thick semicircular canals could indicate a particularly voluminous perilymphatic system that buffers the membranous labyrinth from bathymetric pressure differences, which are most extreme in pelagic deep divers. Possible evidence for the second hypothesis also comes from other pelagic marine reptiles; Neenan *et al.* (2017) reported that pelagic sauropterygians (plesiosaurs) have thicker endosseous semicircular canals than sauropterygian taxa for which the postcranial morphology suggests nearshore habitats (placodonts, nothosaurs and pistosaurs). Although plesiosaurs were viviparous

(O'Keefe & Chiappe, 2011) and therefore not exposed to strong surf while hatchlings, deep diving has been inferred for the group (e.g. Rothschild & Storrs, 2002). The Late Jurassic thalassochelydian turtle *Plesiochelys etalloni*, which has been interpreted to inhabit marine, carbonate platform environments (Billon-Bruyat *et al.*, 2005; Anquetin *et al.*, 2017), has endosseous semicircular canals that are more slender than those of *R. pulchriceps* (Carabajal *et al.*, 2013; Fig. 8). Figure 8 also shows that outside of Chelonioidea, relatively thick canals are present in the testudinoid *Indotestudo elongata* (Blyth, 1854), and our measurements suggest that the semicircular canals of *T. scripta* are not much smaller than those of *R. pulchriceps* (Table 1). Therefore, although thick endosseous semicircular canals appear among all members of the chelonoid total group (protostegids: *R. pulchriceps*; chelonids: e.g. *L. olivacea*; dermochelyids: *Dermochelys coriacea*), the only turtle group that evolved a pelagic lifestyle, and could therefore represent a diving adaptation, the presence of thick canals is not unique to marine turtles.

Georgi & Sipla (2008) also suggested that aquatic reptiles, including turtles, have a lower aspect ratio of the superior division of the labyrinth (i.e. dorsoventrally low semicircular canals but anteroposteriorly elongate canal system) than terrestrial reptiles. However, this hypothesis was based largely on observations of extant reptiles, many of which have a low degree of aquatic adaptation in comparison to extinct secondarily marine Mesozoic reptiles, such as plesiosaurs or mosasaurs. Unlike all living marine reptiles, these Mesozoic groups modified their forelimb autopodia (i.e. phalanges and metacarpals) into rigid paddle-like flippers, whereas sea turtles only have rigid interphalangeal articulations but otherwise flexible forelimb autopodia. Data from these secondarily marine reptiles do not support the hypothesis of

Georgi & Sipla (2008); for example, the mosasaurid *Plioplatecarpus peckensis* Cuthbertson & Holmer, 2015 (Cuthbertson *et al.*, 2015), the thalattosuchian crocodylomorph *Pelagosaurus typus* Bronn, 1841 (Pierce *et al.*, 2017) and the pliosaurid plesiosaur *Peloneustes philarchus* (Seeley, 1869) (Neenan *et al.*, 2017) have superior divisions of the labyrinth with dorsoventrally high aspect ratios. Partial models of ichthyosaur labyrinth endocasts also suggest a relatively dorsoventrally high, anterolaterally short labyrinth morphology (Marek *et al.*, 2015).

In addition, the superior divisions of the labyrinths of *R. pulchriceps* and other sea turtles do not have a low aspect ratio compared with the labyrinths of terrestrial and semiaquatic turtles (Table 2; Fig. 8). We measured aspect ratios for the turtles shown in Figure 8 by dividing the maximal dorsoventral height of the labyrinth (extending from a horizontal mid-plane of the lateral semicircular canal to the maximal dorsal extent of the semicircular canals) by the maximal anteroposterior length. Aspect ratios of chelonoids (including *R. pulchriceps*) are consistently higher (ranging from 0.406 in *Argillochelys cuneiceps* to 0.685 in *Dermochelys coriacea*) than in other turtles considered for this study [ranging from 0.297 in *Lissemys punctata* (Lacépède, 1788) to 0.360 in *Dermatemys mawii* Gray, 1847], with the exception of the terrestrial *I. elongata* (0.452), which falls within the range of measured chelonoids. Indeed, these measurements show that *Dermochelys coriacea*, the extant leatherback sea turtle, has a superior division of the labyrinth with a particularly high aspect ratio (Table 2; Fig. 8).

In summary, our comparative observations indicate that a pelagic lifestyle commonly coincides with the presence of relatively thick endosseous semicircular canals in Reptilia, possibly representing a diving

Table 2. Aspect ratios of endosseous labyrinths of turtles shown in Figure 8

Taxon	Specimen	Endosseous labyrinth length (µm)	Endosseous labyrinth height (µm)	Aspect ratio
† <i>Plesiochelys etalloni</i>	NMB 435	21 127	7173	0.340
<i>Phrynosops geoffroanus</i>	SMF 45470	11 064	3515	0.318
<i>Pleomedusa subrufa</i>	SMF 70504	8090	2636	0.326
<i>Carettochelys insculpta</i>	NHMUK 1903.7.10.1	17 250	5750	0.333
<i>Lissemys punctata</i>	SMF 74141	8546	2541	0.297
<i>Indotestudo elongata</i>	SMF 71585	7639	3456	0.452
<i>Macrochelys temminckii</i>	FMNH 22111	16 150	5560	0.344
<i>Dermatemys mawii</i>	SMF 59463	21 500	7730	0.360
<i>Sternotherus minor</i>	FMNH 211696	7430	2540	0.342
† <i>Rhinocorymbes pulchriceps</i>	CAMSM B55775	10 330	4250	0.411
<i>Dermochelys coriacea</i>	FMNH 171756	28 610	19 600	0.685
† <i>Argillochelys cuneiceps</i>	NHMUK PV R38955	10 105	4103	0.406
<i>Lepidochelys olivacea</i>	SMNS 11070	16 513	6925	0.419

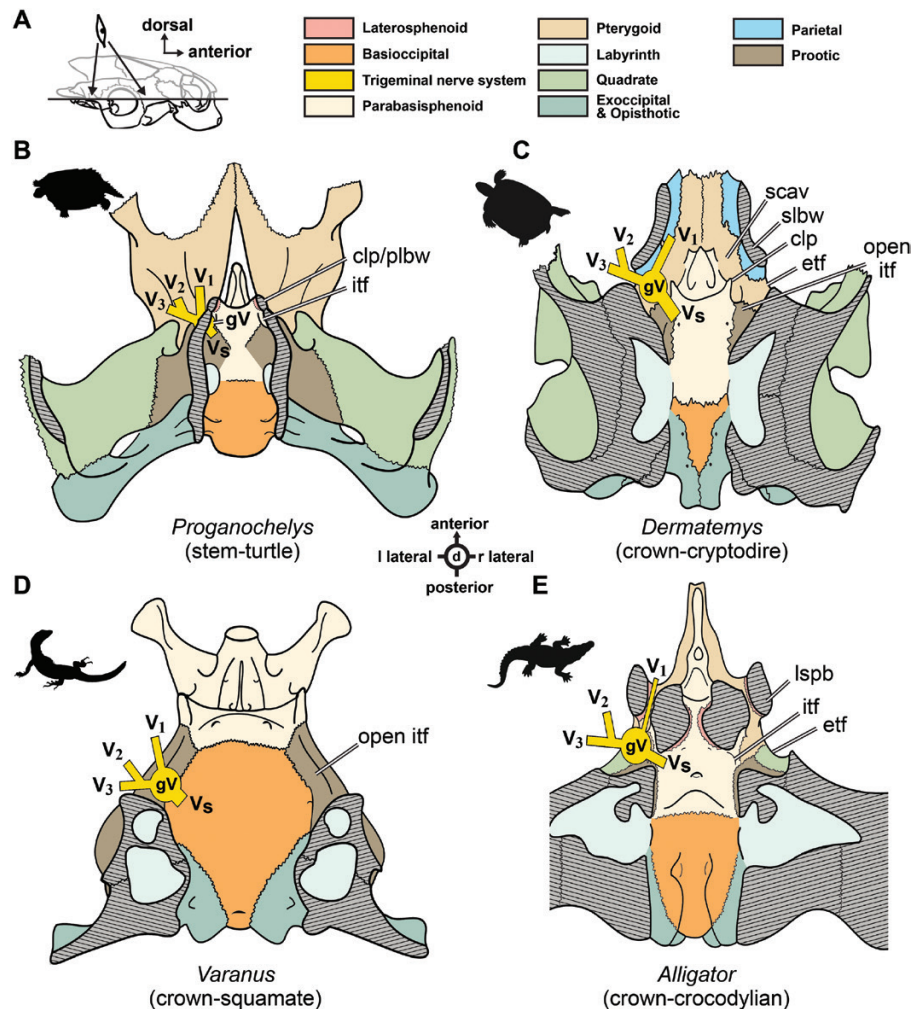


Figure 9. Schematic dorsal views of horizontally sectioned basicrania of selected reptiles. A, schematic view of section used for B–E. B, *Proganochelys quenstedti* (modified from Gaffney, 1990). C, *Dermatemys mawii* (modified from Gaffney, 1979). D, *Varanus indicus* (based on computed tomography scan of AMNH 58389). E, *Alligator mississippiensis* (reconstructed using data from Dufeu & Witmer, 2015). Cross-hatched, grey areas are sectioned skull bones. Silhouettes are from phylopic.org. Abbreviations: clp, clinoid process; etf, external trigeminal foramen; gv, trigeminal ganglion; itf, internal trigeminal foramen; lspb, laterosphenoid bridge; plbw, primary lateral braincase wall; scav, sulcus cavernosus; slbw, secondarily lateral braincase wall; V1, ophthalmic division of trigeminal (cranial nerve V) nerve; V2, maxillary division of trigeminal (cranial nerve V) nerve; V3, mandibular division of trigeminal (cranial nerve V) nerve; Vs, nerve stem of trigeminal (cranial nerve V) nerve.

adaptation. However, the presence of thick canals in the terrestrial *I. elongata* and possibly other non-marine turtles shows that alternative explanations for canal thickness must exist. The hypothesis that aquatic or marine reptiles have semicircular canal systems with low aspect ratios is not supported.

IDENTITY OF THE TRIGEMINAL FORAMEN IN TURTLES

Traditionally, anatomical studies of turtles refer to the skull opening that transmits the maxillomandibular division (CN V₂₋₃) of the trigeminal nerve complex

as the trigeminal foramen (e.g. Gaffney, 1972). However, the term ‘trigeminal foramen’ is potentially misleading within a wider comparative context, when the homology of the cranial structures involved in the formation of the foramen among clades is discussed. This is because of the evolution of the secondary lateral wall of the braincase in turtles. It is generally acknowledged that the ‘trigeminal foramen’ of turtles is not identical (*sensu* Werneburg, 2019, who argues that foramina cannot be homologized) with the trigeminal foramen of other reptiles (e.g. Starck, 1979; Gaffney, 1990; Bhullar & Bever, 2009), because in

turtles the ‘trigeminal foramen’ is positioned within the neomorphic secondary lateral wall of the braincase (e.g. Rieppel, 1993), which is formed primarily by the parietal and the pterygoid (and epipterygoid in non-pleurodiran turtles) (Figs 9C, 10).

The evolution of this part of the braincase can be reconstructed, in part, using evidence from the Late Triassic stem-turtle *Proganochelys quenstedti*. *Proganochelys quenstedti* has a foramen in the primary lateral wall of the braincase (‘prootic foramen’ of Gaffney, 1990; Bhullar & Bever, 2009; but see Lautenschlager *et al.*, 2018), but lacks the neomorphic ‘trigeminal foramen’ (i.e. formed largely by the parietal and pterygoid) of anatomically more modern turtles with a secondary lateral braincase wall (Fig. 9B). The foramen seen in *Proganochelys quenstedti* is formed primarily by the prootic, but dorsally it is bridged by a bone that represents either the laterosphenoid or another ossification of the orbitotemporal region of the chondrocranium (Gaffney, 1990; Bhullar & Bever, 2009; Werneburg & Yaryhin, 2018). This foramen is topologically and anatomically consistent with the morphology and position of the trigeminal foramen in non-turtle reptiles (Fig. 9D, E).

The foramen in *Proganochelys quenstedti* seems to be conserved in some fossil and extant turtles, in which both a medial and a neomorphic lateral foramen coexist (e.g. *Plesiochelys etalloni*, Anquetin *et al.*, 2015; *Pelomedusa subrufa* (Lacépède, 1788), Evers & Benson, 2019). The medial foramen is formed by a bony dorsal bridge that connects the clinoid process of the parabasisphenoid anteriorly with the anterior surface of the prootic posteriorly. The dorsal bridge has been identified as part of the prootic (ossified pila prootica) by Gaffney (1976) and Anquetin *et al.* (2015). In taxa in which both foramina coexist, the nerve stem would have left the brain cavity through the medial foramen, and the trigeminal ganglion becomes laterally encased by the secondary lateral wall of the braincase in a cavum epiptericum (Fig. 10C, D), similar to the condition in mammals (Maier, 1989) and crocodylians (Holliday, 2006). These well-known observations imply that the (medial) trigeminal foramen of anatomically modern turtles is secondarily reduced to a dorsally open notch between the clinoid process anteriorly and the prootic posteriorly (Figs 9C, 10A).

Referring to the neomorphic foramen of anatomically modern turtles as the ‘trigeminal foramen’, as done above in the description of *R. pulchriceps* and most of the comparative turtle literature (e.g. Gaffney, 1979), does have descriptive merit, because parts of the trigeminal division pass through this foramen. Also, this name has been used historically throughout most of the turtle literature. However, to clarify deep homologies between turtles and other reptiles, different names might be more appropriate, specifically

because the ‘prootic foramen’ (*sensu* Gaffney, 1990) in *Proganochelys quenstedti*, or the medial foramen observed in *Plesiochelys etalloni* (Anquetin *et al.*, 2015) and other turtles (Evers & Benson, 2019; Fig. 10C, D), seem to share primary homology with the trigeminal foramen of other reptiles. Several alternative terms have been proposed to highlight the position of the ‘trigeminal foramen’ in the secondary lateral braincase wall of turtles (e.g. foramen otico-parietale, Starck, 1979). Given that only the maxillomandibular rami (CN V₂₋₃) of the trigeminal nerve pass through the foramen, the name maxillomandibular foramen could be adequate, but this term is often used in the crocodile literature (e.g. Sedlmayr, 2002; Holliday & Witmer, 2007), and the neomorphic foramen of turtles is not identical to the similar structure in crocodiles, because the bones forming the foramen differ between these groups. The medial foramen that has been identified so far in only a few turtles could be called a prootic foramen (as described by Gaffney, 1990) or the trigeminal foramen, because it is identical to the foramen for the CN V nerve stem in other reptiles. Here (see Figs 9, 10), we propose the use of the terms ‘internal’ and ‘external’ trigeminal foramen to highlight the evolutionary origin of these structures within Reptilia. According to our observations, only the ‘internal’ trigeminal foramina are identical between clades, whereas squamates lack an ‘external’ trigeminal foramen (Fig. 9D; Evans, 2008), and the ‘external’ foramina of crocodiles (Fig. 8E) and turtles (Fig. 9C) evolved independently.

IMPLICATIONS FOR INTERPRETATING REPTILIAN VESTIBULAR ENDOCASTS

Our comparisons of semicircular canals and ducts in the extant turtle *T. scripta* show that endocasts of endosseous semicircular canals, the sole correlates for the labyrinth organ of extinct species, provide only rough approximations of the underlying membranous structures. Only parts of the posterior and lateral semicircular ducts are reflected by the endosseous cavities. Furthermore, endosseous canals overestimate the diameter and underestimate the length of the membranous structures significantly. However, visible endosseous canals provide approximate measures of some aspects of the shape and geometry of the labyrinth organ, specifically the direction and planar orientations of the membranous semicircular canals. Furthermore, the endosseous anterior semicircular canal reflects the arc length of the membranous anterior semicircular duct reasonably well. Positions of the anterior and lateral ampullae can also be inferred from endocasts of the endosseous labyrinth, whereas the posterior ampulla is concealed by being integrated in a larger

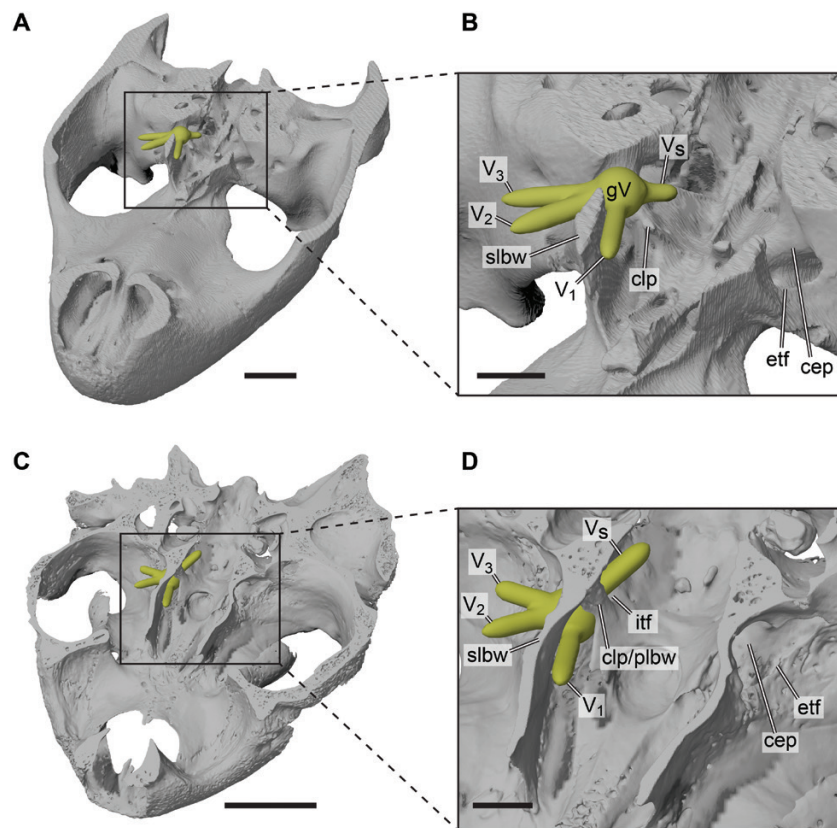


Figure 10. Variation in morphology of the foramina associated with the trigeminal nerve illustrated by three-dimensional renderings of ventral parts of axially sectioned crania. A, B, full cranium and basicranial close-up in anterodorsolateral view of *Chelonia mydas* (NHMUK 1969.776), showing ‘general’ trigeminal configuration of turtles. C, D, full cranium and basicranial close-up in anterodorsolateral view of *Pelomedusa subrufa* (SMF 70504), showing uncommon and possibly plesiomorphic trigeminal configuration, with internal and external ‘trigeminal’ foramina coexisting. Trigeminal nerve is reconstructed in yellow. Abbreviations: cep, cavum epiptericum; clp, clinoid process; etf, external trigeminal foramen; gV, trigeminal ganglion; itf, internal trigeminal foramen; plbw, primary lateral braincase wall; slbw, secondary lateral braincase wall; V₁, ophthalmic division of trigeminal (cranial nerve V) nerve; V₂, maxillary division of trigeminal (cranial nerve V) nerve; V₃, mandibular division of trigeminal (cranial nerve V) nerve; V_s, nerve stem of trigeminal (cranial nerve V) nerve. Scale bars: 20 mm (A); 10 mm (B, C); 3 mm (D).

cavity containing several structures, the secondary common crus. From our small sample of membranous labyrinth models ($N = 1$), it remains unclear whether endosseous canal thickness is proportional to membranous duct thickness.

From these observations, several guidelines for quantitative shape analysis, as commonly executed using 3D geometric morphometrics (e.g. Benson *et al.*, 2017; Neenan *et al.*, 2017; Palci *et al.*, 2017), can be deduced. First, methods that use landmarks on ‘skeletons’ of endosseous semicircular canals, in which the diameter of an endosseous canal is iteratively reduced from the external surface until it is shrunk to a single line of voxels (David *et al.*, 2010), provide a good fit for the position and direction of visible canal portions in some turtles, such as in *T. scripta*. Further work needs to be done to examine the correspondence

of membranous and endosseous labyrinths of taxa in which the latter is extremely thick. However, in a wide range of turtles (see Fig. 8), and more broadly across vertebrates (e.g. birds, Benson *et al.*, 2017; mammals, Ekdale, 2013; Schultz *et al.*, 2017), relatively narrower endosseous semicircular canals are probably indicative of a closer correspondence between canal and duct morphology, similar to the condition in *T. scripta*. For the endosseous anterior semicircular canal, the arc length of the membranous duct can also be estimated adequately by methods using skeletonization. Endosseous canal skeletons also provide better approximations of the length of membranous ducts than methods that place landmarks on the external surface of the endosseous canals, because such methods either overestimate or underestimate the membranous duct length, depending on whether the

dorsal (outer) or ventral (inner) endosseous canal surface is landmarked.

Second, although large portions of the posterior and, particularly, the lateral semicircular canal are concealed in the endosseous labyrinth owing to their course through a common endosseous cavity (secondary common crus), the membranous labyrinth of the extant turtle *T. scripta* shows that membranous labyrinth geometry conforms to the membranous labyrinth morphology that has been reported for other reptiles (e.g. Wever, 1978) and is also identical to gross semicircular canal geometry in mammals (e.g. Gunz *et al.*, 2012; Ekdale, 2013; Pfaff *et al.*, 2015), including Jurassic mammals (e.g. Ruf *et al.*, 2009; Luo *et al.*, 2011), and fishes (e.g. Giles *et al.*, 2018). Therefore, the available data possibly suggest that potentially all gnathostomes share the same spatial relationships of semicircular canal geometry, specifically: (1) that the posterior semicircular duct arches ventrally underneath the posterior section of the lateral semicircular duct, even if this is not visible in the endosseous labyrinth of all taxa; (2) that the anterior and lateral ampullae are always distinguishable in endosseous labyrinths; and (3) that the anterior and posterior semicircular ducts and canals merge into a common crus that is dorsally positioned with regard to the plane of the lateral semicircular duct and canal.

The observation of this generalized labyrinth geometry possibly allows reconstruction of the paths of the posteromedial part of the lateral semicircular canal and the ventromedial part of the posterior semicircular canal in taxa in which both are contained within the same endosseous cavity. Such reconstructions are desirable, because: (1) they represent a closer approximation of the soft tissue anatomy of the vestibular organ than models of the endosseous cavities housing this organ; and (2) they allow more direct comparisons between taxa in which the semicircular canals are completely separated or partly merged in joint endosseous cavities.

Here, we develop a protocol to produce models of isolated semicircular canals for taxa in which portions of the posterior and lateral semicircular canals are enclosed within the same endosseous cavity, the secondary common crus. The respective canal parts are reconstructed by manual manipulation of digital models. Such reconstructions require interpretation of the likely position of the posterior ampulla as a starting point for the posterior semicircular canal. Our model of the membranous labyrinth of *T. scripta*, illustrations of reptilian membranous labyrinths (e.g. Wever, 1978) and comparisons with taxa in which the position of the posterior ampulla can be inferred directly from the endosseous labyrinth (e.g. birds; Benson *et al.*, 2017) indicate that the posterior ampulla is always in a similar position, approximately halfway along the

mediolateral extent of the membranous labyrinth, just dorsally above the level of the deepest ventral extent of the posterior semicircular duct. If the ventral-most extent of the secondary common crus is taken to be indicative of the ventralmost extent of the posterior semicircular duct, the position of the posterior ampulla can be approximated consistently.

For the reconstruction of the lateral semicircular canal, the point at which the lateral semicircular canal connects with the common crus needs to be inferred. Our observations of the membranous labyrinth of *T. scripta*, in addition to endosseous labyrinths in which all semicircular canals are separated from one another (e.g. birds), suggest that the entire lateral semicircular duct lies in a single, flat plane. Therefore, we use a near-horizontal plane placed through the centre of those portions of the lateral semicircular canal that are visible in the endosseous labyrinth model. The point of intersection with the common crus is assumed to be positioned at the intersection of the plane with the common crus. Figure 11 shows a digitally modified model of *T. scripta*, illustrating the reconstruction process outlined above. Using reconstructions like these provides a means for future studies to compile a broad taxonomic sample of reptile ears in comparative shape analyses.

CONCLUSIONS

We provide the first digital models of the neuroanatomical features in a protostegid brain endocast. Our models of the carotid circulation in *R. pulchriceps* show that the right and left cerebral arteries converge within the parabasisphenoid and exit jointly into the sella turcica through a single canal. The 'trigeminal foramen' of turtles is positioned in the secondary lateral wall of the braincase. Comparisons with the Late Triassic stem turtle *Proganochelys quenstedti* and the coexistence of 'internal' and 'external' trigeminal foramina in some turtles demonstrate that the 'trigeminal foramen' of extant turtles is not homologous (or 'identical' *sensu* Werneburg, 2019) to that of other reptiles. The endosseous labyrinth of *R. pulchriceps* has relatively thick semicircular canals and a relatively tall aspect ratio. Comparisons with other turtles and sauropterygians show that thick canals are common in secondarily marine reptiles but are not exclusive to marine animals. The shapes of the labyrinth of *R. pulchriceps* and other secondarily marine reptiles show that low aspect ratios are not indicative of aquatic adaptation, because many extinct marine taxa have dorsoventrally tall labyrinths.

We provide the first comparisons of membranous and endosseous labyrinth shapes, brain tissue and endocasts of the brain cavity based on digital models for turtles. The data from *T. scripta* show that the osteology of the turtle braincase is a poor guide for inferring

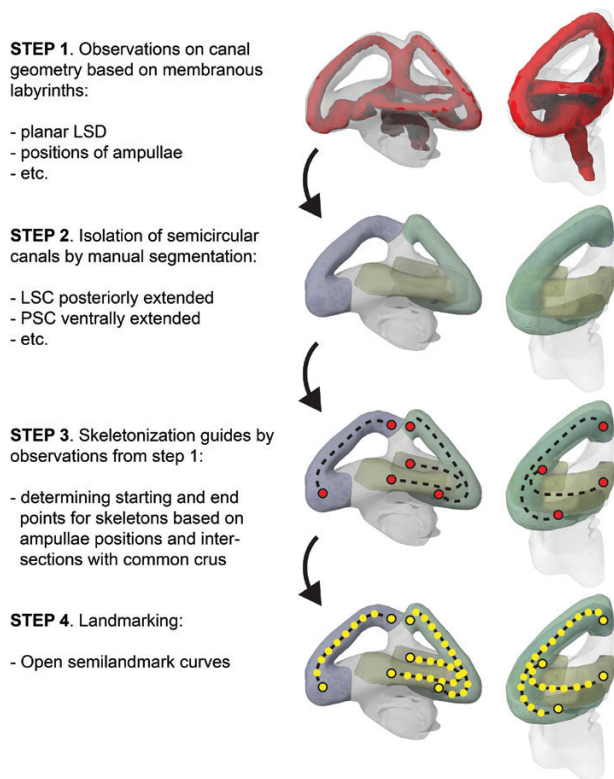


Figure 11. Flow chart illustrating a new method for reconstructing labyrinth morphology from endocasts of the osseous labyrinth. All panels show the left labyrinth of *Trachemys scripta* in dorsal (left) and posterior (right) view. Step 1, observations based on membranous labyrinths provide information about consistent geometric relationships of ducts, which provide the basis for their reconstruction in the absence of soft tissue data, as is the case for fossils. Step 2, the semicircular canals can be 'isolated' from a model of an endosseous labyrinth. Portions of canals that are confluent with one another (e.g. when a secondary common crus is present, as in most turtles) are extended based on observations from membranous labyrinths. For example, the lateral semicircular canal is extended posteriorly to reflect duct morphology better. Step 3, skeletonization of semicircular canal models. The canal diameter is successively shrunk until it forms a line of single voxels. Beginning and end points of skeletons are determined based on ampullae positions and duct intersections with the common crus, which are inferred from the general observations from step 1. The canal skeletons are now approximate representations of the membranous duct morphology and can be validated by comparisons with real duct morphology, if available, as is the case here for *T. scripta*. Step 4, the skeletons of the endosseous semicircular canals can now be landmarked, using open semilandmark curves. Abbreviations: LSC, lateral semicircular canal; LSD, lateral semicircular duct; PSC, posterior semicircular canal.

brain shape. Likewise, the endosseous labyrinth is a particularly poor representation of the membranous labyrinth, owing to partly merged posterior and lateral semicircular canals in a secondary common crus and owing to a mismatch of semicircular duct and canal thickness. It is currently unclear whether endosseous semicircular canal thickness is correlated with semicircular duct thickness. Comparative data from turtles with thick endosseous semicircular canals, such as chelonoids, are necessary to test these relationships and to investigate their potential ecological signal.

The membranous labyrinths of *T. scripta* show that the general geometry of canals conforms to that of all gnathostomes; although semicircular duct geometry is sometimes confounded by the geometry of endosseous cavities such as the secondary common crus, which forms a single pathway for parts of the lateral and posterior semicircular ducts, the relative paths of the semicircular ducts seem to be the same even in distantly related groups, such as mammals. However, comparative semicircular duct data of more taxa are necessary to scrutinize our observations further. Generalized relationships of the canal courses allow the approximate reconstruction of canal sections that are merged in the endosseous cavities, which will allow future quantitative comparisons between turtles and other vertebrates.

ACKNOWLEDGEMENTS

This research was supported by a Natural Environment Research Council (NERC) studentship to S.W.E. on the Doctoral Training Partnership (DTP) Environmental Research (NE/L0021612/1) and received further support from the SYNTHESYS Project (<http://www.synthesys.info/>), which is financed by European Community Research Infrastructure Action under the FP7 'Capacities' Program (grant awarded to S.W.E.). J.M.N. was supported by a Leverhulme Early Career Fellowship (ECF-2017-360). G.S.F. was supported by two Fundação de Amparo à Pesquisa do Estado de São Paulo (FAPESP) grants, numbers 2014/25379-5 and 2016/03934-2. I.W. was supported by Deutsche Forschungsgemeinschaft (DFG)-grant WE 544/6-1. We thank all the curators who granted access to specimens under their care, particularly Matt Riley (Sedgwick Museum, Cambridge, UK), Sandra Chapman (The Natural History Museum, London, UK) and Rainer Schoch (Staatliches Museum für Naturkunde Stuttgart, Stuttgart, Germany). We thank Farah Ahmed (The Natural History Museum, London, UK) for assistance with the scanning of *R. pulchriceps*, and Yi Hongyu for sharing the CT scan of *Varanus*

indicus for comparisons. We also thank Gilles Laurent (Max Planck Institute for Brain Research, Frankfurt, Germany) and Russell Jacobs (USC Keck School of Medicine, Los Angeles, CA, USA) for acquiring the scan of *T. scripta*, and G. Laurent for sharing the data with us. We are thankful to Torsten Scheyer (Paläontologisches Institut und Museum, Universität Zürich, Zurich, Switzerland) for making us aware of the *T. scripta* scan. We also acknowledge phylopic.org, from which the silhouettes used in Figure 9 are taken. We are thankful for helpful and constructive reviews by Juliana Sterli, Stephan Lautenschlager and an anonymous reviewer, which greatly improved an earlier version of this manuscript.

REFERENCES

- Albrecht PW. 1967.** The cranial arteries and cranial arterial foramina of the turtle genera *Chrysemys*, *Sternotherus*, and *Trionyx*: a comparative study with analysis of possible evolutionary implications. *Tulane Studies in Zoology* **14**: 81–99.
- Albrecht PW. 1976.** The cranial arteries of turtles and their evolutionary significance. *Journal of Morphology* **149**: 159–182.
- Anquetin J, Püntener C, Billon-Bruyat J-P. 2015.** *Portlandemys gracilis* n. sp., a new coastal marine turtle from the Late Jurassic of Porrentruy (Switzerland) and a reconsideration of plesiochelyid cranial anatomy. *PLoS ONE* **10**: e0129193.
- Anquetin J, Püntener C, Joyce WG. 2017.** A review of the fossil record of turtles of the clade Thalassocheyleia. *Bulletin of the Peabody Museum of Natural History* **58**: 317–369.
- Baird IL. 1970.** The anatomy of the reptilian ear. In: Gans C, Parsons TS, eds. *Biology of the Reptilia. Volume 2. Morphology B*. London: Academic Press, 193–275.
- Baird IL. 1974.** Anatomical features of the inner ear in submammalian vertebrates. In: Keidel WD, Neff WD, eds. *Handbook of sensory physiology, volume V/1: auditory system: anatomy physiology (ear)*. Berlin: Springer-Verlag, 159–212.
- Balanoff AM, Bever GS, Colbert MW, Clarke JA, Field DJ, Gignac PM, Ksepka DT, Ridgely RC, Smith NA, Torres CR, Walsh S, Witmer LM. 2015.** Best practices for digitally constructing endocranial casts: exemplified from birds and their dinosaurian relatives. *Journal of Anatomy* **229**: 173–190.
- Balanoff AM, Bever GS, Rowe TB, Norell MA. 2013.** Evolutionary origins of the avian brain. *Nature* **501**: 93–96.
- Benson RB, Starmer-Jones E, Close RA, Walsh SA. 2017.** Comparative analysis of vestibular ecomorphology in birds. *Journal of Anatomy* **231**: 990–1018.
- Berlin JC, Kirk EC, Rowe TB. 2013.** Functional implications of ubiquitous semicircular canal non-orthogonality in mammals. *PLoS ONE* **8**: e79585.
- Bever GS, Lyson TR, Field DJ, Bhullar B-AS. 2015.** Evolutionary origin of the turtle skull. *Nature* **525**: 239–242.
- Bhullar B-AS, Bever GS. 2009.** An archosaur-like laterosphenoid in early turtles (Reptilia: Pantestudines). *Breviora* **518**: 1–11.
- Billon-Bruyat J-P, Lécuyer C, Martineau F, Mazin J-M. 2005.** Oxygen isotope compositions of Late Jurassic vertebrate remains from lithographic limestones of western Europe: implications for the ecology of fish, turtles, and crocodilians. *Palaeogeography, Palaeoclimatology, Palaeoecology* **216**: 359–375.
- Brinkman DB, Hart M, Jamniczky H, Colbert M. 2006.** *Nichollsemys baieri* gen. et sp. nov., a primitive chelonoid turtle from the Late Campanian of North America. *Paludicola* **5**: 111–124.
- Cadena E, Parham JF. 2015.** Oldest known marine turtle? A new protostegid from the Lower Cretaceous of Colombia. *PaleoBios* **32**: 1–421.
- Carabajal AP, Sterli J, Georgi J, Poropar SF, Kear BP. 2017.** Comparative neuroanatomy of extinct horned turtles (Meiolaniidae) and extant terrestrial turtles (Testudinidae), with comments on the palaeobiological implications of selected endocranial features. *Zoological Journal of the Linnean Society* **180**: 930–950.
- Carabajal AP, Sterli J, Müller J, Hilger A. 2013.** Neuroanatomy of the marine Jurassic turtle *Plesiochelys etalloni* (Testudinata, Plesiochelyidae). *PLoS ONE* **8**: e69264.
- Christensen-Dalsgaard J, Brandt C, Willis KL, Christensen CB, Ketten D, Edds-Walton P, Fay RR, Madsen PT, Carr CE. 2012.** Specialisation for underwater hearing by the tympanic middle ear of the turtle, *Trachemys scripta elegans*. *Proceedings of the Royal Society B: Biological Sciences* **279**: 2816–2824.
- Clack JA. 2016.** Vertebrate diversity in a sensory system: the fossil record of otic evolution. In: Clack JA, Fay RR, Popper AN, eds. *Springer handbook of auditory research, V. 59: evolution of the vertebrate ear: evidence from the fossil record*. Cham: Springer International Publishing, 1–16.
- Codorniu L, Carabajal AP, Pol D, Unwin D, Rauhut OWM. 2016.** A Jurassic pterosaur from Patagonia and the origin of the pterodactyloid neurocranium. *PeerJ* **4**: e2311.
- Cuthbertson RS, Maddin HC, Holmes RB, Anderson JS. 2015.** The braincase and endosseous labyrinth of *Plioplatecarpus peckensis* (Mosasauridae, Plioplatecarpinae), with functional implications for locomotor behavior. *The Anatomical Record* **298**: 1597–1611.
- David R, Droulez J, Allain R, Berthoz A, Janvier P, Bennequin D. 2010.** Motion from the past. A new method to infer vestibular capacities of extinct species. *Comptes Rendus Palevol* **9**: 397–410.
- Dufeu DL, Witmer LM. 2015.** Ontogeny of the middle-ear air-sinus system in Alligator mississippiensis (Archosauria: Crocodylia). *PLoS One* **10**: e0137060, Dryad Digital Repository, doi.org/10.5061/dryad/7h853 (data).
- Edinger T. 1929.** Die fossilen Gehirne. *Ergebnisse der Anatomie und Entwicklungsgeschichte* **28**: 1–249.

- Ekdale EG. 2013.** Comparative anatomy of the bony labyrinth (inner ear) of placental mammals. *PLoS One* **8**: e66624.
- Ekdale EG. 2016.** Form and function of the mammalian inner ear. *Journal of Anatomy* **228**: 324–337.
- Evans S. 2008.** The skull of Lepidosauria. In: Gans C, Gaunt AS, Adler K, eds. *Biology of the Reptilia, volume 20, morphology H*. London: Academic Press, 1–347.
- Evers SW, Barrett PM, Benson RBJ. 2018.** Project: *Rhinochelys* CT data and 3D models. *MorphoSource*. Available at: http://www.morphosource.org/Detail/ProjectDetail/Show/project_id/581
- Evers SW, Barrett PM, Benson RBJ. 2019.** Anatomy of *Rhinochelys pulchriiceps* (Protostegidae) and marine adaptations during the early evolution of chelonioidea. *PeerJ* **7**: e6811.
- Evers SW, Benson RBJ. 2018.** Project: turtle CT data and 3D models. *MorphoSource*. Available at: http://www.morphosource.org/Detail/ProjectDetail/Show/project_id/462
- Evers SW, Benson RBJ. 2019.** A new phylogenetic hypothesis of turtles with implications for the number of evolutionary transitions to marine lifestyles supports an Early Cretaceous origin and rapid diversification of Chelonioidea. *Palaeontology* **62**: 93–134.
- Ferreira GS, Iori FV, Hermanson G, Langer MC. 2018.** New turtle remains from the Late Cretaceous of Monte Alto-SP, Brazil, including cranial osteology, neuroanatomy and phylogenetic position of a new taxon. *Paläontologische Zeitschrift* **92**: 481–498.
- Friedman M, Giles S. 2016.** Actinopterygians: the ray-finned fishes – an explosion of diversity. In: Clack JA, Fay RR, Popper AN, eds. *Springer handbook of auditory research, V. 59: evolution of the vertebrate ear: evidence from the fossil record*. Cham: Springer International Publishing, 17–49.
- Gaffney ES. 1972.** An illustrated glossary of turtle skull nomenclature. *American Museum Novitates* **2486**: 1–33.
- Gaffney ES. 1975a.** A phylogeny and classification of the higher categories of turtles. *Bulletin of the American Museum of Natural History* **155**: 391–436.
- Gaffney ES. 1975b.** A taxonomic revision of the Jurassic turtles *Portlandemys* and *Plesiochelys*. *American Museum Novitates* **2574**: 1–19.
- Gaffney ES. 1976.** Cranial morphology of the European Jurassic turtles *Portlandemys* and *Plesiochelys*. *Bulletin of the American Museum of Natural History* **157**: 487–544.
- Gaffney ES. 1977.** An endocranial cast of the side-necked turtle, *Bothremys*, with a new reconstruction of the palate. *American Museum Novitates* **2639**: 1–12.
- Gaffney ES. 1979.** Comparative cranial morphology of recent and fossil turtles. *Bulletin of the American Museum of Natural History* **164**: 65–376.
- Gaffney ES. 1982.** Cranial morphology of the baenid turtles. *American Museum Novitates* **2737**: 1–22.
- Gaffney ES. 1983.** The cranial morphology of the extinct horned turtle *Meiolania platyceps*, from the Pleistocene of Lord Howe Island, Australia. *Bulletin of the American Museum of Natural History* **175**: 364–479.
- Gaffney ES. 1990.** The comparative osteology of the Triassic turtle *Proganochelys*. *Bulletin of the American Museum of Natural History* **194**: 1–176.
- Gaffney ES. 1992.** *Ninjemys*, a new name for “*Meiolania*” *oweni* (Woodward), a horned turtle from the Pleistocene of Queensland. *American Museum Novitates* **3049**: 1–10.
- Gaffney ES, Zangerl R. 1968.** A revision of the chelonian genus *Bothremys* (Pleurodira: Pelomedusidae). *Fieldiana, Geology Memoirs* **16**: 193–239.
- Georgi JA. 2008.** Semicircular canal morphology as evidence of locomotor environment in amniotes. Unpublished PhD Thesis, Stony Brook University.
- Georgi JA, Sipla JS. 2008.** Comparative and functional anatomy of balance in aquatic reptiles and birds. In: Thewissen JHM, Nummela S, eds. *Sensory evolution on the threshold, adaptations in secondarily aquatic vertebrates*. Berkeley: University of California Press, 133–256.
- Giles S, Rogers M, Friedman M. 2018.** Bony labyrinth morphology in neopterygian fishes (Actinopterygii: Neopterygii). *Journal of Morphology* **279**: 426–440.
- Gunz P, Ramsier M, Kuhrig M, Hublin J-J, Spoor F. 2012.** The mammalian bony labyrinth reconsidered, introducing a comprehensive geometric morphometric approach. *Journal of Anatomy* **220**: 529–543.
- Henson OW. 1974.** Comparative anatomy of the middle ear. In: Keidel WD, Neff WD, eds. *Handbook of sensory physiology, volume V/1: auditory system: anatomy physiology (ear)*. Berlin: Springer-Verlag, 40–110.
- Hetherington T. 2008.** Comparative anatomy and function of hearing in aquatic amphibians, reptiles, and birds. In: Thewissen JHM, Nummela S, eds. *Sensory evolution on the threshold, adaptations in secondarily aquatic vertebrates*. Berkeley: University of California Press, 183–209.
- Higuchi S, Sugahara F, Pascual-Anaya J, Takagi W, Oisi Y, Kuratani S. 2018.** Inner ear development in cyclostomes and evolution of the vertebrate semicircular canals. *Nature* **565**: 347–350.
- Hirayama R. 1998.** Oldest known sea turtle. *Nature* **392**: 705–708.
- Holliday CM. 2006.** *Evolution and function of the jaw musculature and adductor chamber of Archosaurs (crocodilians, dinosaurs, and birds)*. Unpublished PhD Thesis, Ohio University Athens.
- Holliday CM, Witmer LM. 2007.** Archosaur adductor chamber evolution: integration of musculoskeletal and topological criteria in jaw muscle homology. *Journal of Morphology* **268**: 457–484.
- Hooks GE. 1998.** Systematic revision of the Protostegidae, with a redescription of *Calcarichelys gemma* Zangerl, 1953. *Journal of Vertebrate Paleontology* **18**: 85–98.
- Hopson JA. 1979.** Paleoneurology. In: Gans C, Northcutt RG, Uliński P, eds. *Biology of the Reptilia, Volume 9*. London: Academic Press, 39–146.
- Jamniczky HA. 2008.** Turtle carotid circulation: a character analysis case study. *Biological Journal of the Linnean Society* **93**: 239–256.

- Jamniczky HA, Russel AP. 2007.** Reappraisal of patterns of nonmarine cryptodiran turtle carotid circulation: evidence from osteological correlates and soft tissues. *Journal of Morphology* **268**: 571–587.
- Jones MEH, Werneburg I, Curtis N, Penrose R, O'Higgins P, Fagan MJ, Evans SE. 2012.** The head and neck anatomy of sea turtles (Cryptodira: Chelonioida) and skull shape in Testudines. *PLoS ONE* **7**: e47852.
- Joyce WG. 2007.** Phylogenetic relationships of Mesozoic turtles. *Bulletin of the Peabody Museum of Natural History* **48**: 3–102.
- Joyce WG, Volpato VS, Rollot Y. 2018.** The skull of the carettochelyid turtle *Anosteira pulchra* from the Eocene (Uintan) of Wyoming and the carotid canal system of carettochelyid turtles. *Fossil Record* **21**: 301–310.
- Kardong KV. 2008.** *Vertebrates: comparative anatomy, function, evolution*, 2nd edn. New York: WCB/McGraw-Hill.
- Kear BP, Lee MSY. 2006.** A primitive protostegid from Australia and early sea turtle evolution. *Biology Letters* **2**: 116–119.
- Lautenschlager S, Butler RJ. 2016.** Neural and endocranial anatomy of Triassic phytosaurian reptiles and convergence with fossil and modern crocodylians. *PeerJ* **4**: e2251.
- Lautenschlager S, Ferreira GS, Werneburg I. 2018.** Sensory evolution and ecology of early turtles revealed by digital endocranial reconstructions. *Frontiers in Ecology and Evolution* **6**: 7.
- Lipka TR, Therrien F, Weishampel DB, Jamniczky HA, Joyce WG, Colbert MW, Brinkman DB. 2006.** A new turtle from the Arundel Clay facies (Potomac Formation, Early Cretaceous) of Maryland, U.S.A. *Journal of Vertebrate Paleontology* **26**: 300–307.
- Luo Z-X, Ruf I, Schultz JA, Martin T. 2011.** Fossil evidence on evolution of inner ear cochlea in Jurassic mammals. *Proceedings of the Royal Society B: Biological Sciences* **278**: 28–34.
- Maier W. 1989.** Ala temporalis and alisphenoid in therian mammals. In: Splechtna H, Hilgers H, eds. *Trends in vertebrate morphology. Progress in zoology* 35. Stuttgart: Fischer Verlag, 396–400.
- Marek RD, Moon BC, Williams M, Benton MJ. 2015.** The skull and endocranium of a Lower Jurassic ichthyosaur based on digital reconstructions. *Palaeontology* **58**: 723–742.
- Martínez RDF, Lamanna MC, Novas FE, Ridgely RC, Casal GA, Martínez JE, Vita JR, Witmer LM. 2016.** A basal lithostrotian iitanosaur (Dinosauria: Sauropoda) with a complete skull: implications for the evolution and paleobiology of Titanosauria. *PLoS ONE* **11**: e0151661.
- McDowell SB Jr. 1961.** On the major arterial canals in the ear-region of testudinoid turtles and the classification of the Testudinoidea. *Bulletin of the Museum of Comparative Zoology* **125**: 21–40.
- Miyashita T. 2012.** Chapter 7. Geometric and developmental perspectives on the evolution of the skull and internal carotid circulation in turtles. In: Brinkman DB, Holroyd PA, Gardner JD, eds. *Morphology and evolution of turtles, vertebrate paleobiology and paleoanthropology series*. Dordrecht: Springer, 71–101.
- Müller J, Sterli S, Anquetin J. 2011.** Carotid circulation in amniotes and its implications for turtle relationships. *Neues Jahrbuch für Geologie und Paläontologie-Abhandlungen* **261**: 289–297.
- Myers TS, Polcyn MJ, Mateus O, Vineyard DP, Gonçalves AO, Jacobs LL. 2018.** A new durophagous stem cheloniid turtle from the Lower Paleocene of Cabinda, Angola. *Papers in Palaeontology* **4**: 161–176.
- Neenan JM, Reich T, Evers SW, Druckenmiller PS, Voeten DFAE, Choiniere JN, Barrett PM, Pierce SE, Benson RBJ. 2017.** Evolution of the sauropterygian labyrinth with increasingly pelagic lifestyles. *Current Biology* **27**: 3852–3858.
- Nick L. 1912.** Das Kopfskelet von *Dermochelys coriacea* L. *Zoologische Jahrbücher, Abteilung für Anatomie und Ontogenie der Tiere* **33**: 431–552.
- O'Keefe FR, Chiappe LM. 2011.** Viviparity and K-selected life history in a Mesozoic marine plesiosaur (Reptilia, Sauropterygia). *Science* **333**: 870–873.
- Palci A, Hutchinson MN, Caldwell MW, Lee MSY. 2017.** The morphology of the inner ear of squamates and its bearing on the origin of snakes. *Royal Society Open Science* **4**: 170685.
- Parsons TS. 1970.** The nose and Jacobson's organ. In: Carl G, Parsons TS, eds. *Biology of the Reptilia, Volume 2, morphology B*. London: Academic Press, 99–191.
- Pfaff C, Czerny S, Nagel D, Kriwet J. 2017.** Functional morphological adaptations of the bony labyrinth in marsupials (Mammalia, Theria). *Journal of Morphology* **278**: 742–749.
- Pfaff C, Martin T, Ruf I. 2015.** Bony labyrinth morphometry indicates locomotor adaptations in the squirrel-related clade (Rodentia, Mammalia). *Proceedings of the Royal Society B: Biological Sciences* **282**: 20150744.
- Pierce SE, Williams M, Benson RBJ. 2017.** Virtual reconstruction of the endocranial anatomy of the Early Jurassic marine crocodylomorph *Pelagosaurus typus* (Thalattosuchia). *PeerJ* **5**: e3225.
- Porter WR, Sedlmayr JC, Witmer LM. 2016.** Vascular patterns in the heads of crocodylians: blood vessels and sites of thermal exchange. *Journal of Anatomy* **229**: 800–824.
- Porter WR, Witmer LM. 2015.** Vascular patterns in iguanas and other squamates: blood vessels and sites of thermal exchange. *PLoS ONE* **10**: e0139215.
- Rabi M, Zhou C-F, Wings O, Ge S, Joyce WG. 2013.** A new xinjiangchelyid turtle from the Middle Jurassic of Xinjiang, China and the evolution of the basipterygoid process in Mesozoic turtles. *BMC Evolutionary Biology* **13**: 203.
- Raselli I. 2018.** Comparative cranial morphology of the Late Cretaceous protostegid sea turtle *Desmatochelys lowii*. *PeerJ* **6**: e5964.
- Retzius G. 1884.** *Das Gehörorgan der Wirbelthiere, Vol. 2: Das Gehörorgan der Reptilien, der Vögel und der Säugethiere*. Stockholm: Samson & Wallin.

- Rieppel O. 1993.** Patterns of diversity in the reptilian skull. In: Hanken J, Hall BK, eds. *The skull, volume 2, patterns of structural and systematic diversity*. Chicago: The University of Chicago Press, 344–390.
- Rollot Y, Lyson TR, Joyce WG. 2018.** A description of the skull of *Eubaena cephalica* (Hay, 1904) and new insights into the cranial circulation and innervation of baenid turtles. *Journal of Vertebrate Paleontology* **38**: e1474886.
- Rothschild BM, Storrs GW. 2002.** Decompression syndrome in plesiosaurs (Sauropterygia: Reptilia). *Journal of Vertebrate Paleontology* **23**: 324–328.
- Rowe TB, Macrini TE, Luo Z-X. 2011.** Fossil evidence on the origin of the mammalian brain. *Science* **332**: 955–957.
- Ruf I, Luo Z-X, Wible JR, Martin T. 2009.** Petrosal anatomy and inner ear structures of the Late Jurassic *Henkelotherium* (Mammalia, Cladotheria, Dryolestidae): insight into the early evolution of the ear region in cladotherian mammals. *Journal of Anatomy* **214**: 679–693.
- Schoch RR, Anderson JS. 2016.** Amphibia: a case of diversity and convergence in the auditory region. In: Clack JA, Fay RR, Popper AN, eds. *Springer handbook of auditory research, V. 59: evolution of the vertebrate ear: evidence from the fossil record*. Cham: Springer International Publishing, 17–49.
- Schultz JA, Zeller U, Luo X-Z. 2017.** Inner ear labyrinth anatomy of monotremes and implications for mammalian inner ear evolution. *Journal of Morphology* **278**: 236–263.
- Schumacher GH. 1972.** *Die Kopf- und Halsregion der Lederschildkröte Dermochelys coriacea (LINNAEUS 1766) – Anatomische Untersuchungen im Vergleich zu anderen rezenten Schildkröten*. Berlin: Akademie-Verlag.
- Schwenk K. 2008.** Comparative anatomy and physiology of chemical senses in nonavian aquatic reptiles. In: Thewissen JHM, Nummela S, eds. *Sensory evolution on the threshold, adaptations in secondarily aquatic vertebrates*. Berkeley: University of California Press, 65–81.
- Sedlmayr JC. 2002.** *Anatomy, evolution, and functional significance of cephalic vasculature in Archosaurs*. Unpublished PhD Thesis, Ohio University Athens.
- Soliman MA. 1964.** Die Kopfnerven der Schildkröten. *Zeitschrift für Wissenschaftliche Zoologie* **169**: 216–312.
- Spoor F, Garland G Jr, Krovitz G, Ryan TM, Silcox MT, Walker A. 2007.** The primate semicircular canal system and locomotion. *Proceedings of the National Academy of Sciences of the United States of America* **104**: 10808–10812.
- Spoor F, Zonneveld F. 1998.** Comparative review of the human bony labyrinth. *Yearbook of Physical Anthropology* **41**: 211–251.
- Starck D. 1979.** Cranio-cerebral relations in recent reptiles. In: Gans C, Northcutt RG, Ulinski P, eds. *Biology of the Reptilia, Volume 9, Neurology A*. London: Academic Press, 1–38.
- Sterli J, De la Fuente MS. 2010.** Anatomy of *Condorchelys antiqua* Sterli, 2008, and the origin of the modern jaw closure mechanism in turtles. *Journal of Vertebrate Paleontology* **30**: 351–366.
- Sterli J, Müller J, Anquetin J, Hilger A. 2010.** The parabasisphenoid complex in Mesozoic turtles and the evolution of the testudinate basicranium. *Canadian Journal of Earth Sciences* **47**: 1337–1346.
- Thewissen JHM, Nummela S. 2008.** *Sensory evolution on the threshold, adaptations in secondarily aquatic vertebrates*. Berkeley: University of California Press.
- Tong H, Hirayama R, Makhoul E, Escuillie F. 2006.** *Rhinochelys* (Chelonioidea: Protostegidae) from the Late Cretaceous (Cenomanian) of Nammoura, Libanon. *Società Italiana di Scienze Naturali e del Museo Civico di Storia Naturale di Milano* **147**: 113–138.
- Tulenok FJ, Sheil CA. 2007.** Formation of the chondrocranium of *Trachemys scripta* (Reptilia: Testudines: Emydidae) and a comparison with other described turtle taxa. *Journal of Morphology* **268**: 127–151.
- Walsh SA, Barrett PM, Milner AC, Manley G, Witmer LM. 2009.** Inner ear anatomy is a proxy for deducing auditory capability and behaviour in reptiles and birds. *Proceedings of the Royal Society B: Biological Sciences* **276**: 1355–1360.
- Werneburg I. 2019.** Morphofunctional categories and ontogenetic origin of temporal skull openings in amniotes. *Frontiers in Earth Sciences* **7**: 13.
- Werneburg I, Maier W. 2019.** Diverging development of akinetic skulls in cryptodire and pleurodire turtles: an ontogenetic and phylogenetic study. *Vertebrate Zoology* **69**: 113–143.
- Werneburg I, Yaryhin O. 2018.** Character definition and tempus optimum in comparative chondrocranial research. *Acta Zoologica* **00**: 1–13.
- Wever EG. 1978.** *The reptile ear*. Princeton: Princeton University Press.
- Willis KL, Christensen-Dalsgaard J, Ketten DR, Carr CE. 2013.** Middle ear cavity morphology is consistent with an aquatic origin for Testudines. *PLoS ONE* **8**: e54086.
- Wilson VJ, Melville Jones G. 1979.** *Mammalian vestibular physiology*. New York: Plenum Press.
- Witmer LM, Chatterjee S, Franzosa J, Rowe T. 2003.** Neuroanatomy of flying reptiles and implications for flight, posture and behaviour. *Nature* **425**: 950–953.
- Witmer LM, Ridgely RC, Dufeu DL, Semones MC. 2008.** Using CT to peer into the past: 3D visualization of the brain and ear regions of birds, crocodiles, and nonavian dinosaurs. In: Endo H, Frey R, eds. *Anatomical imaging. Towards a new morphology*. Tokyo: Springer, 67–87.
- Wyneken J. 2001.** The anatomy of sea turtles. *U.S. Department of Commerce NOAA Technical Memorandum NMFS-SEF-470*: 1–172.
- Yaryhin O, Werneburg I. 2018.** Tracing the developmental origin of a lizard skull: chondrocranial architecture, heterochrony, and variation in lacertids. *Journal of Morphology* **279**: 1058–1087.
- Yi H, Norell MA. 2015.** The burrowing origin of modern snakes. *Science Advances* **1**: e1500743.
- Zangerl R. 1960.** The vertebrate fauna of the Selma Formation of Alabama. Part V. An advanced chelonid sea turtle. *Fieldiana, Geology Memoirs* **3**: 281–312.